



This is a repository copy of *Two-site recognition of Staphylococcus aureus peptidoglycan by lysostaphin SH3b*.

White Rose Research Online URL for this paper:
<https://eprints.whiterose.ac.uk/153806/>

Version: Accepted Version

Article:

Gonzalez-Delgado, L.S., Walters-Morgan, H., Salamaga, B. et al. (7 more authors) (2020) Two-site recognition of Staphylococcus aureus peptidoglycan by lysostaphin SH3b. *Nature Chemical Biology*, 16 (1). pp. 24-30. ISSN 1552-4450

<https://doi.org/10.1038/s41589-019-0393-4>

This is a post-peer-review, pre-copyedit version of an article published in *Nature Chemical Biology*. The final authenticated version is available online at:
<http://dx.doi.org/10.1038/s41589-019-0393-4>.

Reuse

Items deposited in White Rose Research Online are protected by copyright, with all rights reserved unless indicated otherwise. They may be downloaded and/or printed for private study, or other acts as permitted by national copyright laws. The publisher or other rights holders may allow further reproduction and re-use of the full text version. This is indicated by the licence information on the White Rose Research Online record for the item.

Takedown

If you consider content in White Rose Research Online to be in breach of UK law, please notify us by emailing eprints@whiterose.ac.uk including the URL of the record and the reason for the withdrawal request.



eprints@whiterose.ac.uk
<https://eprints.whiterose.ac.uk/>

1
2
3
4
5
6
7
8
9
10
11
12
13
14
15
16
17
18
19
20
21
22
23
24
25
26
27
28

Two site recognition of *Staphylococcus aureus* peptidoglycan by lysostaphin SH3b

Luz S. Gonzalez-Delgado^{1,2†}, Hannah Waters-Morgan^{3†}, Bartłomiej Salamaga^{1,2}, Angus J
Robertson^{1,2}, Andrea M. Hounslow^{1,2}, Elżbieta Jagielska⁴, Izabela Sabala⁴,
Mike P. Williamson^{1,2*}, Andrew L. Lovering^{3*} and Stéphane Mesnage^{1,2*}

¹ Department of Molecular Biology and Biotechnology, University of Sheffield, Firth Court,
Western Bank, Sheffield, UK;

² Krebs Institute, University of Sheffield, Firth Court, Western Bank, Sheffield, UK;

³ Institute of Microbiology and Infection & School of Biosciences, University of
Birmingham, Birmingham, UK

⁴ International Institute of Molecular and Cell Biology, Warsaw, Poland

† These authors contributed equally to this work

* Corresponding authors

Email: s.mesnage@sheffield.ac.uk; m.williamson@sheffield.ac.uk; a.lovering@bham.ac.uk

Short title: Peptidoglycan recognition by lysostaphin

29 **Abstract (150 words)**

30 Lysostaphin is a bacteriolytic enzyme targeting peptidoglycan, the essential component of the
31 bacterial cell envelope. It displays a very potent and specific activity towards staphylococci,
32 including methicillin-resistant *Staphylococcus aureus* (MRSA). Lysostaphin causes rapid cell
33 lysis and disrupts biofilms, and is therefore a therapeutic agent of choice to eradicate
34 staphylococcal infections. The C-terminal SH3b domain of lysostaphin recognizes
35 peptidoglycans containing a pentaglycine crossbridge and has been proposed to drive the
36 preferential digestion of staphylococcal cell walls. Here, we elucidate the molecular
37 mechanism underpinning recognition of staphylococcal peptidoglycan by the lysostaphin
38 SH3b domain. We show that the pentaglycine crossbridge and the peptide stem are recognized
39 by two independent binding sites located on opposite sides of the SH3b domain, thereby
40 inducing a clustering of SH3b domains. We propose that this unusual binding mechanism
41 allows a synergistic and structurally dynamic recognition of *S. aureus* peptidoglycan and
42 underpins the potent bacteriolytic activity of this enzyme.

43 Introduction

44 Lysostaphin is a bacteriolytic enzyme produced and secreted by *Staphylococcus simulans*
45 biovar *staphylolyticus*¹. This exotoxin has a potent activity against a wide range of
46 staphylococci including the opportunistic nosocomial pathogen *Staphylococcus aureus*². It
47 displays endopeptidase activity and cleaves the pentaglycine crossbridges present in the
48 essential component of the bacterial cell wall (peptidoglycan), leading to rapid cell lysis. In *S.*
49 *simulans* biovar *staphylolyticus*, immunity to lysostaphin is conferred by Lif, an aminoacyl
50 transferase that introduces serine residues into peptidoglycan crossbridges³. This modification
51 dramatically reduces susceptibility to lysostaphin.

52 Due to its powerful antistaphylococcal activity against both planktonic cells and biofilms⁴,
53 lysostaphin has been extensively studied as a therapeutic agent to treat infections caused by
54 methicillin resistant *S. aureus* (MRSA)⁵⁻¹¹. Recent studies have reported the design of
55 lysostaphin variants with a reduced antigenicity and enhanced therapeutic efficacy^{12,13} as well
56 as strategies to harness the bactericidal activity of this toxin¹⁴⁻¹⁶. Collectively, the studies
57 published have demonstrated that lysostaphin represents a credible therapeutic agent to combat
58 staphylococcal infections, either alone or in combination with antibiotics¹⁷.

59 Lysostaphin is a modular hydrolase produced as a pre-proenzyme. It comprises a signal
60 peptide, 15 N-terminal repeats of 13 amino acids, a catalytic domain with glycylglycyl
61 endopeptidase activity and a C-terminal peptidoglycan binding domain of 92 residues³. The
62 specificity of lysostaphin towards staphylococci has been attributed to its binding domain,
63 which recognizes pentaglycine crossbridges^{18,19}. Recent crystallographic studies have
64 confirmed early models and showed that the pentaglycine stem is recognized by a shallow
65 groove formed between strands $\beta 1$ - $\beta 2$ and the RT loop, the binding specificity being essentially
66 conferred by steric hindrance²⁰. Despite this exquisite recognition mechanism, the SH3b
67 domain displays a very weak affinity for the pentaglycine stems and binding has been shown
68 to be optimal with multimeric peptidoglycan fragments, suggesting a mechanism more
69 complex than initially anticipated^{20,21}.

70 Here, we combine NMR and X-ray crystallography to elucidate the mechanism underpinning
71 the recognition of staphylococcal peptidoglycans by the lysostaphin SH3b domain. We show
72 that the SH3b domain contains two binding sites located on opposite sides of the protein,
73 allowing a mutually exclusive recognition of these two peptidoglycan moieties. The
74 recognition of the pentaglycine crossbridge and the peptide stem is therefore shared by two
75 independent SH3b domains, allowing protein clustering on the peptidoglycan. We propose that

76 the combination of low affinity and high off-rate binding results in a synergistic and structurally
77 dynamic binding that is particularly suitable for the recognition of non-contiguous epitopes of
78 mature, physiological peptidoglycan. This unusual mechanism underpins the potent activity of
79 lysostaphin and its capacity to punch holes in the cell walls to cause rapid cell lysis.

80

81 **Results**

82

83 **NMR analysis of SH3b-peptidoglycan interactions**

84 We sought to investigate the mechanism underpinning SH3b-PG interaction using NMR
85 titrations with a panel of ligands of increasing complexity. Six ligands were produced, either
86 by solid-phase synthesis or purified from *S. aureus* PG following digestion by hydrolytic
87 enzymes (Supplementary Fig. 1). The ligands tested corresponded to a tetrasaccharide
88 (GlcNAc-MurNAc- GlcNAc-MurNAc; GMGM), a pentaglycine crossbridge (GGGGG; G5),
89 a tetrapeptide stem (A γ QKA; P4), a tetrapeptide with the pentaglycine as a lateral chain
90 (A γ QK[GGGGG]A; P4-G5), a disaccharide-peptide dimer (GlcNAc-MurNAc-
91 A γ QK[GGGGG]AA- GlcNAc-MurNAc-A γ QK[GGGGG]A; (GM-P4-G5)₂) and the peptide
92 A γ QK[GGGGG]AA-A γ QKA (P5-G5-P4) containing two peptide stems crosslinked via a
93 single pentaglycine crossbridge.

94 Complete resonance assignment of the doubly labelled SH3b domain was obtained using
95 standard triple resonance experiments (Supplementary Fig. 2). The six ligands were used to
96 measure chemical shift perturbations (CSPs) associated with main-chain and side-chain amides
97 (Supplementary Fig. 3 and Supplementary Table 1).

98 In agreement with previous studies, our results showed that pentaglycine (G5) peptides interact
99 with several residues located in a narrow cleft corresponding to the binding groove originally
100 proposed for *Staphylococcus capitis* ALE-1, a close homolog of Lss. These included residues
101 N405 to Y411, T429, G430, M453, D456 and Y472 (Fig. 1a, Supplementary Fig. 3a). CSPs of
102 the signals corresponding to SH3b residues following addition of this ligand indicated a fast
103 exchange rate with a weak binding affinity in the millimolar range ($K_D=890 \pm 160\mu\text{M}$).

104 *S. aureus* peptidoglycan is highly crosslinked and therefore contains mostly tetrapeptide stems
105 (P4). The SH3b domain bound to P4 peptides with a fast exchange rate and a low affinity
106 ($K_D=963 \pm 198\mu\text{M}$), suggesting that this minimal ligand (like the G5 peptide) is not the
107 complete PG motif recognised by the SH3b domain. Surprisingly, residues presenting
108 pronounced chemical shifts upon binding to the P4 ligand were located on the side of the
109 protein opposite to the G5 binding cleft (*e.g.*, N421, I425, A443, V440; Fig. 1b and
110 Supplementary Fig. 3b). Residue R427 side chain also showed a significant CSP. Two
111 hydrophobic residues presenting relatively large CSPs were buried in the structure, suggesting
112 that they were not directly in contact with the P4 ligand (V461 and L473). This observation

113 implies that whereas binding at G5 is fairly rigid lock-and-key, binding at P4 is more of an
114 induced fit interaction, with adaptation of the protein to fit its ligand.

115 As expected, a tighter binding was observed for two PG monomer ligands made of the
116 tetrapeptide stem with a pentaglycine lateral chain alone (P4-G5; $K_D = 98 \pm 42 \mu\text{M}$). The most
117 prominent CSPs corresponded to residues previously identified with the simple ligands G5 and
118 P4 in both cases (Fig. 1b,c). Several residues broadened and disappeared with the P4-G5 ligand
119 (N405, I425, V461, G462, Y472 and L473), indicating a slow to medium exchange rate
120 (Supplementary Fig. 3c). Titrations with a synthetic tetrasaccharide (GlcNAc-MurNac)₂
121 revealed no interactions between the protein and the synthetic disaccharides, suggesting that
122 the sugars do not play a key role in the recognition of peptidoglycan by the SH3b domain.

123 Next, we studied the binding of SH3b domain to dimeric PG fragments made of two peptide
124 stems crosslinked by a pentaglycine chain. One of these ligands contained a single pentaglycine
125 chain (P5-G5-P4), whilst the other had two (GM-P5-G5-GM-P4-G5). The largest CSPs
126 associated with binding were those previously identified with simpler ligands (G5 and P4) (Fig.
127 1e,f and Supplementary Fig. 3e,f). The CSPs corresponding to the recognition of the P4/P5 or
128 G5 moieties were typical of a fast exchange rate, with an affinity of $100 \pm 34 \mu\text{M}$ for the P5-
129 G5-P4 ligand. In the case of the most complex ligand (GM-P5-G5-GM-P4-G5), we could not
130 determine any binding affinity since the protein started to precipitate in the presence of 4
131 equivalents of ligand resulting in the disappearance of the signals. One surface residues (W489)
132 located close to residues binding the peptide stem only displayed CSPs with dimeric ligands.
133 Interestingly, the CSPs observed for the larger ligands had fewer large changes than were seen
134 for the simpler ligands (Supplementary Fig. 3).

135 Collectively, NMR titrations suggested that the SH3b domain recognises both the PG peptide
136 stems and crossbridges via distinct sets of residues located on opposite sides of the protein
137 surface.

138

139

140 Structure of the SH3b-*S. aureus* PG peptide stem complex

141 We attempted to co-crystallize the SH3b domain with a branched P4-G5 ligand and were
142 successful in obtaining crystals that diffracted to 1.4 Å resolution. Our initial expectation was
143 to observe this ligand binding to the surface of a single SH3b domain but upon solving the
144 structure it was apparent that the G5 was recognized by one domain and P4 by another
145 (symmetry-related copy) as shown in Fig. 2. The 1.4 Å high resolution, synchrotron set is able
146 to trace three of the P4 units (γ QKA representing units 2-4) and a lower 2.5 Å home source set

147 is essentially identical but allows tracing of the full P4 ligand (A γ QKA). In our structures, the
148 pentaglycine bridge sits identically to that of other SH3b structures (5LEO), but then projects
149 the crossbridge link (K to G5) and stem peptide (A γ QKA) into a pocket located on the opposite
150 side of a second SH3b monomer (Fig. 2a-c). The two SH3 domains make no strong interactions
151 with one another, but display a shape/surface complementarity that allows for close contact
152 around the shared ligand.

153 The P4 and G5 components of the ligand are at approximately 90° angles to one another, and
154 the carbon atoms of the K3 sidechain make favourable contacts with the hydrophobic
155 sidechains of Y407, T422', I424' and W489' (prime used to denote opposing SH3b). Units one
156 to three of the P4 peptidoglycan stem display a linear β -like conformation, with peptide bonds
157 hydrogen-bonding to residues from both SH3b domains: γ Q2 NH to carbonyl of K406, K3 NH
158 to carbonyl of D423', and K3 CO to NH of I425'. This arrangement makes for much stronger
159 contacts of the SH3b domains to P3/P4 in comparison to P1/P2, and would place the attached
160 physiological peptidoglycan saccharide units at the edge of both monomers. There is a clearly
161 defined pocket for the terminal D-Ala 4 (Fig. 2d), with the COO- group making a salt-bridge
162 to the sidechain of R427', and a hydrophobic pocket comprised of I424', I425', R433', H458',
163 W460', P474' and W489' surrounding the methyl sidechain of the substrate. Sequence and
164 structure alignments between lysostaphin SH3b (SH3_5) and other proteins indicate that the
165 P4 D-Ala-carboxylate pocket is likely a conserved feature of wider superfamily members
166 (Supplementary Fig. 4), with relevance for both SH3_3 and SH3_4 subgroups. There are no
167 current structures for the latter, but the two SH3_4 domains of *Clostridium* phage lysin
168 phiSM101 each have a carboxylate ligand bound at this position, suggesting an important role
169 for the residues equivalent to lysostaphin R427²².

170

171 **Mutational analysis of the binding activity**

172 We sought to confirm the contribution of the SH3b residues identified by NMR and X-ray
173 crystallography to the recognition of the crossbridge (G5) and peptide stem (P4) ligands. Six
174 single-site substitution mutant domains were produced and analysed by NMR (N405A,
175 M453A, Y472S, I425A, R427M, W489L). ¹⁵N HSQC spectra of all mutant domains revealed
176 that these were properly folded, allowing us to measure CSP values in the presence of the
177 maximum concentration of ligand previously used (32 equivalents). As expected, all mutations
178 were associated with a reduction in CSPs when compared to the wild-type domain
179 (Supplementary Fig. 5). We characterised the reduction in binding affinity using a figure of

180 residual binding, which is defined as the ratio of chemical shift changes of mutant to WT,
181 averaged over all amino acids. Given the weak binding affinities, and the fact that the protein
182 concentration is always lower than the affinity, these correspond roughly to the expected
183 reduction in affinity. Domains with mutations in the residues involved in the interaction with
184 G5 still retained a relatively high residual binding, the N405A mutation having the most
185 pronounced effect (16% residual binding for the N405A mutant, 55.5% for M453A and 24.6%
186 for Y472S). Whilst the I425 still displayed 29.4% residual binding, the mutations R427M and
187 W489L had a major impact on binding to the P4 ligand (1.6% and 6.6% residual binding,
188 respectively). These results confirmed the contribution of the residues identified by NMR and
189 crystallography to the binding of minimal ligands. The limited impact of most of the mutations
190 studied on binding is in agreement with the X-ray and NMR results which revealed that the
191 recognition of peptidoglycan fragments by SH3b domains relies on a complex network of
192 interactions.

193

194 **Binding of SH3b derivatives to purified PG sacculi**

195 Due to the labour-intensive nature of NMR analyses and the fact that these analyses are limited
196 to study interactions with soluble substrates, we designed a quantitative *in vitro* binding assay
197 with peptidoglycan sacculi which represent the natural substrate of lysostaphin. The SH3b
198 domain was fused to the monomeric fluorescent protein mNeonGreen²³ to follow binding in
199 the presence of increasing amount of peptidoglycan (Fig. 3 and Supplementary Table 2).
200 Recombinant proteins were purified using two chromatography steps including metal affinity
201 and gel filtration. As a first step we measured the binding of SH3b-mNeonGreen fusions to
202 peptidoglycan purified from the WT, *femB* and *femAB* mutants (containing five, three and one
203 glycine residue in crossbridges, respectively) (Fig. 3a and Supplementary Fig. 6). As expected,
204 binding occurred in a dose-dependent manner and binding to the *femB* mutant was clearly
205 reduced (1.71-fold change), whilst a more drastic reduction in binding was observed with the
206 *femAB* mutant (2.20-fold change). The residual, dose-dependent binding to the *fem* mutant
207 peptidoglycans is in agreement with our identification of a second site recognizing the peptide
208 stems. Fifteen recombinant fusions with mutations in residues previously identified were
209 purified and their binding activity was measured (Fig. 3b,c and Supplementary Fig. 6). Most
210 of the mutations clearly impaired binding to peptidoglycan to a level similar to the level of
211 binding displayed by the WT-mNeonGreen fusion to the *femB* peptidoglycan. The biggest
212 impact on binding was observed with mutations R427M and W489L impairing the recognition
213 of peptide stems (2.47- and 2.18-fold changes as compared to the WT, respectively). These

214 results therefore confirmed the role of the residues identified by NMR and X-ray
215 crystallography and provided the first evidence that peptide stem recognition by the lysostaphin
216 SH3b domain is critical for binding.

217

218 **Impact of SH3b mutations on Lss activity**

219 The SH3b mutations previously described (Supplementary Fig. 6) were introduced into the
220 mature lysostaphin enzyme. Recombinant proteins were purified and serial 2-fold dilutions
221 were spotted on agar plates containing autoclaved *S. aureus* cells as a substrate (Supplementary
222 Fig. 7). The enzymatic activity was detected as a clearing zone resulting from the solubilisation
223 of *S. aureus* cell walls. Four independent series of protein purifications were carried out, each
224 including a wild-type lysostaphin protein. One lysostaphin mutant (Lss_M453A) showing an
225 aberrant circular dichroism spectrum could not be analysed; mutant R427M was also excluded
226 from the study as it did not bind to the nickel column. Amongst all the mutations tested, Y472S
227 and W489L led to the most important effects observed (9-fold decrease), whilst all the others
228 had only a limited impact. These results were in line with the binding assays, indicating that
229 no single mutation abolished enzymatic activity and supported our results indicating that the
230 recognition of the peptide stem is equally, if not more, important for binding and activity as is
231 binding to the pentaglycine bridge.

232 **Discussion**

233 The crystal structure reported here shows that SH3b has two well-defined binding sites for *S.*
234 *aureus* peptidoglycan: a narrow groove that accommodates the G5 lateral chain, with a tightly
235 defined geometry and thus little tolerance for amino acid variants; and a more open site for the
236 P4 peptide stem. One might therefore expect that the specificity for *S. aureus* PG arises entirely
237 from the G5 site, which should be critical for binding. This is not what is indicated by the other
238 results reported here.

239 The interpretation of CSPs, and of the affinities determined by fitting CSPs to a saturation
240 curve, is more complex than may at first appear. A perturbation of an ^{15}N or ^1H nuclear
241 shielding is typically caused by a change in the chemical environment at the nucleus, for
242 example due to a change in hydrogen bonding or a change in the position of neighboring
243 functional groups. Hydrogen bonding is highly directional, implying that an increased mobility
244 of a ligand within its binding site will result in significantly smaller CSPs. Increased mobility
245 will not necessarily result in weaker overall binding, because the loss in enthalpy due to a
246 weaker time-averaged hydrogen bond can easily be compensated by a gain in entropy. Smaller
247 CSPs can therefore indicate a more dynamic binding interaction, rather than simply weaker
248 binding. This phenomenon matches what is observed here (Supplementary Fig. 3). With a
249 simple G5 or P4 ligand that binds in a single site, there are some large CSPs, clearly defining
250 the location of the site (Supplementary Fig. 3a,b). With larger ligands, although the affinity is
251 stronger (implying cooperative binding at both sites, see below), there are fewer large CSP
252 values. The most obvious interpretation is that within each site the ligand has greater mobility,
253 presumably because the physical linkage between the G5 and P4 groups prevents the larger
254 ligands from binding optimally in both sites simultaneously.

255 There have been many analyses published of binding affinities of ligands that interact via two
256 different sites. A powerful approach is the concept of effective concentration^{24,25}. Consider a
257 ligand L1-L2 that binds at two sites, R1 and R2, with a flexible linker between L1 and L2 (Fig
258 4a). If the ligand detaches from site R2, then the rate at which L2 rebinds at R2 is given by
259 $k_{\text{on}} \times [\text{L2}]_{\text{eff}}$, where k_{on} is the rate constant for binding and $[\text{L2}]_{\text{eff}}$ is the effective concentration
260 of L2 at the R2 binding site (Fig 4b). For a short linker with optimal length and geometry,
261 $[\text{L2}]_{\text{eff}}$ can be orders of magnitude larger than $[\text{L2}]$, leading to much stronger binding than
262 would be seen in the absence of L1 (because the overall affinity for L2 is equal to the off-rate
263 divided by the on-rate, and we can assume that the off-rate is unaffected by the presence of the
264 linker): in other words, to cooperative binding, such that the affinity for the intact ligand L1-
265 L2 is much stronger than the affinity for L1 or L2 alone. Conversely, if the linker is too short

266 (Fig 4c), then L2 is unable to reach R2, and $[L2]_{\text{eff}}$ is smaller than $[L2]$, leading to a complete
267 lack of cooperativity. If the binding sites R1 and R2 allow for some flexibility in geometry,
268 then we may have a situation as shown in Fig 4d, where binding of the ligand can be achieved
269 by allowing some mobility in the bound conformation at the cost of suboptimal binding
270 geometry. The cooperativity will not be as great as it would be with ideal geometry and thus
271 the affinity will be stronger but not by a large amount. This appears to be exactly the situation
272 observed here: affinity is 10× stronger, but CSPs are smaller. Furthermore, single site mutations
273 have relatively little effect on the affinity or on enzymatic activity, suggesting that the exact
274 shape or complementarity of the binding site is relatively unimportant, consistent with this
275 model.

276 It is a legitimate question to ask why SH3b should have evolved separate binding sites for G5
277 and P4, but located on the protein surface in such a way that simultaneous binding to both sites
278 is not possible. What is the biological advantage? Our data, and the interpretation derived here,
279 provide suggestions. The function of the SH3b domain is to attach lysostaphin to PG, in such
280 a way as to increase access of the catalytic domain to its G5 substrate. It is therefore not
281 desirable for the affinity for PG to be too strong, otherwise SH3b would detach too slowly and
282 not allow the catalytic domain to move from one G5 substrate to another. A good solution is to
283 have two binding sites, both with weak affinity and thus rapid off-rates, and organised so as to
284 provide a moderate degree of cooperativity in binding to the complex substrate. This allows
285 the protein to ‘walk’ around the PG surface, continually keeping at least one site bound, but
286 permitting rapid searching on the PG surface. A very similar solution has been adopted by a
287 number of cellulases, which have two different cellulose binding domains arranged in tandem
288 ²⁶⁻²⁹.

289 A comparison of interactions at the two sites with different ligands (Fig. 1) suggests that the
290 larger ligands have weaker interactions at the G5 site, since the G5 interactions (red) decrease
291 more than do the P4 interactions (green). This result is at first sight counterintuitive, because
292 the lysostaphin catalytic domain specifically targets G5. However SH3b should not bind too
293 tightly to G5, because otherwise it would block access of the catalytic domain. It therefore
294 makes sense for the larger (and thus more cell-wall-like) fragments to favor binding of the
295 peptide stem, as long as some specificity for G5 is maintained, and as long as SH3b is not
296 locked into binding at any particular location. We may therefore describe the role of SH3b as
297 to contribute to the initial (weak) binding of the enzyme on the PG surface. This conclusion is
298 also consistent with the observation that the mutations more critical to binding affinity are
299 found in the P4 site, not the G5 site. Surprisingly, and in agreement with this result, the SH3b

300 domain still binds in a dose-dependent manner to the *femAB* peptidoglycan, containing
301 crossbridges made of a single glycine residue. This suggests that the recognition of the
302 pentaglycine stem is not essential for the binding of the enzyme with its substrate. Based on
303 this result, it is tempting to hypothesize that the catalytic activity of lysostaphin rather than the
304 binding itself is the major determinant for the specific hydrolysis of staphylococcal
305 peptidoglycan. In *Staphylococcus carnosus*, the *femB* mutation is associated with a 3000-fold
306 increase in the MIC values for lysostaphin from 0.01 to 32 $\mu\text{g/ml}$ ³⁰. Given the limited impact
307 of the SH3b mutations on binding, this result suggests that the high resistance to lysostaphin in
308 the *femB* mutant is not caused by the slight difference in binding activity of the penta- vs tri-
309 glycine interpeptide bridge, but is mainly due to the decreased enzymatic activity of
310 lysostaphin.

311 The networks of contacts between ligand and two sets of SH3 domains strongly suggest that
312 our two-site model for P4-G5 (and therefore true, complex sacculus ligand) is physiologically
313 relevant. The observed pocket for the terminal P4 D-Ala is highly complementary in both shape
314 and contact type; a lack of adjoining pocket for a second D-Ala of a pentapeptide is in keeping
315 with the dominance of tetrapeptides in staphylococcal peptidoglycan ³¹. Residues responsible
316 for P4 recognition are conserved in several homologues present in the PDB despite the relative
317 low sequence identity across the entire domain – *S. capitis* ALE-1 (code 1R77, 83% sequence
318 identity, ¹⁹), *Staphylococcus* phage GH15 lysin (2MK5, 49%, ³²) and phage phi7917 lysin
319 (5D76, 30%, unpublished). These related structures have features that validate our
320 identification of the P4 binding site (overlays shown in Supplementary Fig. 4): in ALE-1 a
321 purification tag places a lysine in an identical position to the K3 crosslink, and in phi7917 a
322 muramyl dipeptide cleavage product has bound in this region. Our identification of a “second”
323 binding site supplementing the “traditional” pentaglycine cleft may have implications for other
324 SH3b and SH3-like domains that are used in varying architectures to recognize peptidoglycan
325 in organisms that do not utilize the G5 crossbridge.

326 No major difference exists between the structure of the SH3b domain in its apo form (4LXC)
327 and in complex with the P4-G5 ligand (this work), suggesting that the ligand displays a
328 dynamic structure to “fit” within the binding clefts present on the SH3b domain. Previous NMR
329 studies support this idea and have shown that the D-Lac, L-Ala, and D-Glu adopt a limited
330 number of conformers, whereas the L-Lys-D-Ala termini are disordered (with no NOE contacts
331 observed ³³). Further relaxation measurements using the P4-G5 ligand could be carried out to
332 test this hypothesis but it appears difficult to extrapolate relaxation experiments to a complex
333 molecule such as peptidoglycan.

334 The data presented here provide an explanation as to why the binding activity of the SH3b
335 domain of lysostaphin is not affected by exogenous pentaglycine or its own catalytic
336 products²¹; our model suggests that the mucopeptide interactions are only satisfied when
337 presented by non-contiguous epitopes of mature, physiological peptidoglycan. The location of
338 these sites on different faces of the SH3b molecule ensures that both are unlikely to be
339 contacted by a soluble, torsionally less-restricted fragment. We hypothesize that this will be an
340 excellent method for processive degradation of the peptidoglycan.

341 The structure of the SH3b domain in complex with the P4-G5 peptide shed light on the NMR
342 analyses previously published³⁴ and those described in this manuscript, revealing the existence
343 of two independent binding sites on opposite sides of the SH3b domain. The binding
344 mechanism described here is consistent with the formation of large protein aggregates during
345 titration with complex PG fragments. Recognition of the same PG peptide stem by independent
346 SH3b domains (referred to as “clustering”) leads to an effective increase in enzyme
347 concentration at the cell surface. In agreement with this hypothesis, the direct observation of
348 *S. aureus* cell wall digestion by lysostaphin using atomic force microscopy revealed the
349 existence of nanoscale perforations that precede cell lysis³⁵.

350

351 Materials and methods

352

353 Bacterial strains, plasmids and growth conditions.

354 Bacterial strains and plasmids used in this study are described in Supplementary Table 3. *E.*
355 *coli* Lemo21 (DE3) and NEB5 α strains were grown at 37°C in Luria-Bertani (LB) or M9
356 minimal medium containing 1 g/L of ¹⁵NH₄Cl (and 2 g/L ¹³C₆-glucose where necessary),
357 supplemented with ampicillin at a concentration of 100 μ g/ml.

358

359 Construction of recombinant plasmids for protein production.

360 Both plasmids expressing the full length lysostaphin (pET-Lss) and the SH3b domains with a
361 non-cleavable N-terminal His-tag for NMR studies (pET-SH3b) have been previously
362 described ^{36,37}. The plasmid encoding the SH3b-mNeonGreen fusion (pET-SH3b-NG) was
363 constructed by Gibson assembly using a DNA synthetic fragment (Integrated DNA
364 Technology) cloned into the vector pET2818 cut with NcoI and BamHI. Plasmid pET-SH3b-
365 TEV used to produce the SH3b domain without a tag for X-ray crystallography was constructed by
366 Gibson assembly using a synthetic DNA fragment (Integrated DNA Technology) cloned into
367 pET2817 digested with NcoI and BamHI. The amino acid sequences of the wild-type
368 recombinant proteins are described in Supplementary Fig 8.

369

370 Site-directed mutagenesis.

371 Mutagenesis of plasmids pET-SH3b and pET-Lss was performed using the GeneArt® Site-
372 Directed Mutagenesis System (Thermo Fisher Scientific). All primers used in this study are
373 described in the Supplementary Table 4. The same pair of oligonucleotides was used to
374 introduce mutations in both plasmids, except for mutations N405D and W489L which required
375 distinct pairs of oligonucleotides to build mNeonGreen fusions and lysostaphin mutants.

376

377 Purification of recombinant Lss protein and Lss-SH3b protein domains.

378 Cells were grown to an optical density at 600nm (OD₆₀₀) of 0.7 in LB or M9 media for NMR
379 analyses and protein production was induced by the addition of 1 mM IPTG. After 4h, induced
380 cells were harvested and resuspended in buffer A (50 mM Tris-HCl, 500m M NaCl, pH 8.0)
381 and crude lysates were obtained by sonication (3 \times 30s, 20% output; Branson Sonifier 450).
382 Soluble proteins were loaded onto a HiTrap IMAC column (GE Healthcare, Uppsala, Sweden)
383 charged with Ni²⁺ or Zn²⁺ ions for SH3b (alone or fused to mNeonGreen) and full-length

384 lysostaphin, respectively. His-tagged proteins were eluted with a 20 column volume linear
385 gradient of buffer B (500 mM imidazole, 50 mM Tris-HCl, 500 mM NaCl, pH 8.0).
386 Recombinant His-tagged proteins were concentrated and purified by size-exclusion
387 chromatography on a Superdex 75 HR column (GE Healthcare, Uppsala, Sweden). For NMR
388 experiments, proteins were purified using 50 mM Na₂HPO₄ (pH 6.0). All purified proteins were
389 analysed by SDS-PAGE.

390 For crystallography experiments, the SH3b domain was produced using plasmid pET-SH3b-TEV.
391 The N-terminal tag was removed using recombinant TEV protease (0.5 mg of TEV per mg of
392 SH3b protein). Digestions were performed at 37°C overnight in buffer C (150 mM NaCl, 50
393 mM Tris-HCl, pH 8.35). Following digestion, proteins were loaded onto a HiTrap IMAC
394 column, and cleaved SH3b proteins were recovered in the flow through. Proteins
395 concentrations were determined using absorbance at 280 nm.

396 The characterization of all recombinant proteins is described in the supplementary information
397 section (Supplementary Fig. 8-12).

398

399 **Purification of *S. aureus* PG sacculi**

400 PG sacculi were isolated from exponentially growing *S. aureus* cells as previously described
401 ³⁸. Pure PG was freeze-dried and resuspended at a final concentration of 25 mg/ml.

402

403 **Peptidoglycan digestions for NMR titration assays**

404 *S. aureus* PG was digested with mutanolysin (Sigma). To purify PG dimers (GM-P5-G5-GM-
405 P4-G5), 180 mg of PG were digested with 2.5 mg of mutanolysin in a final volume of 5 ml
406 using 20 mM phosphate buffer (pH 6.0). After overnight incubation the enzyme was heat-
407 inactivated. Half of the sample was used to purify dimers. The pH of the other half of digestion
408 was adjusted to 7.5 and it was further digested with 2 mg of EnpA to generate disaccharide-
409 peptides. EnpA was heat-inactivated.

410

411 **Purification of peptidoglycan fragments by rp-HPLC**

412 Prior to rp-HPLC analysis and fractionation, soluble peptidoglycan fragments were reduced
413 with sodium borohydride to eliminate double peaks corresponding to the α - and β -anomers as
414 previously described ³⁸. Fractionation of material corresponding to the digestion of 50 mg of
415 PG was carried out on a Hypersil GOLD aQ column (C18; 21 × 250 mm, Thermo Scientific)
416 and separated at a flow rate of 10 ml/min using 10 mM ammonium phosphate (pH 5.5) as a

417 mobile phase (buffer A). After a short isocratic step (2 column volumes), PG fragments were
418 eluted with a 15 column volume methanol linear gradient (0 to 30%) in buffer A. Individual
419 peaks were collected, freeze-dried and analysed by mass spectrometry. The fractions
420 corresponding to the major dimer (GM-P5-G5-GM-P4-G5) were desalted by HPLC using a
421 water-acetonitrile gradient, freeze-dried and resuspended in MilliQ water.

422

423 **Production of peptidoglycan fragments by chemical synthesis**

424 The tetrasaccharide (GMGM) was described previously³⁹. All peptides and branched peptides
425 (>95% purity) were purchased from Peptide Protein Research Ltd. (UK) Purity was assessed
426 by HPLC and mass spectrometry. The characterization of all ligands is described in the
427 supplementary information section. The pentaglycine peptide was purchased from SIGMA
428 Aldrich (ref. G5755).

429

430

431 **Crystallography and structure determination**

432 Crystallisation was initiated via standard screening in sitting drop 96-well clover-leaf
433 crystallography trays at 18 mg/ml with 3.41 mM A γ QK[GGGGG]A in a 1:2 drop ratio of screening
434 agent to protein solution. The trays were incubated at 18 °C. Tetragonal bipyramidal crystals
435 formed within the first 48 hours in 100 mM Bis-tris pH 5.5, 25% (w/v) poly-ethylene glycol 3350
436 and 200 mM ammonium sulphate.

437 Crystals were cryo-protected using the above conditions (inclusive of A γ QK[GGGGG]A to
438 maintain the ligand:protein complex), and an additional 20% v/v ethylene glycol. Two datasets
439 were collected (Supplementary Table 5): a high resolution set at the I03 beamline, Diamond Light
440 Source, Oxford, and a second set on a Rigaku Micromax home source. Data were processed with
441 XiaII/XDS⁴⁰. The B-factors for the high-resolution set are higher than expected, but match that
442 of the Wilson B, and the dataset has a normal intensity distribution. An initial model was solved
443 using the existing apo structure 5LEO²⁰ as a molecular replacement model in PHASER⁴¹, and the
444 corresponding structure autobuilt using PHENIX⁴², with the ligand added via visual inspection of
445 the difference map. The structure was updated and refined using COOT⁴³, PHENIX⁴² and PDB-
446 redo⁴⁴, resulting in a final structure with an R/Rfree of 19.9%/23.0%.

447

448 **NMR experiments**

449 NMR experiments were conducted on Bruker Avance I 800 and DRX-600 spectrometers at
450 298K. 2D NHSQC experiments were carried out using the b_hsqctf3gpsi pulse program

451 (Bruker) with relaxation delay 1 s, 128 complex increments (ca. 1 h 18 m per spectrum). Lys-
452 SH3b proteins were quantified by measuring the absorbance at 280 nm and adjusted to a
453 concentration of 60 μ M in 50 mM Na₂HPO₄ (pH 6.0). All ligands were quantified by NMR
454 based on the intensity of methyl protons using trimethylsilylpropanoic acid (TSP) as a standard.
455 ¹⁵N HSQC experiments and chemical shift perturbation (CSP) analyses were performed as
456 previously described ³⁹.

457

458 **PG binding assays**

459 The PG binding activity of SH3b domains was studied using in-gel fluorescence. Protein
460 amounts equivalent to 3 μ g of the wild-type recombinant SH3b-mNeonGreen were adjusted
461 based on the fluorescence intensity of the bands corresponding to the full length proteins.
462 Following incubation in the presence of increasing amounts of PG (0-400 μ g) in a final volume
463 of 40 μ l for 20 min at room temperature, PG and bound proteins were pelleted at 17,000 \times g
464 for 5 minutes. Twenty μ l of supernatant corresponding to unbound proteins were loaded on an
465 SDS-PAGE and scanned using a BioRad Chemidoc XRS+ system. Fluorescence intensity was
466 quantified using the ImageJ software. The percentage of binding was determined using the
467 signal intensity measured in the absence of PG as a reference.

468

469 **Lysostaphin activity assays**

470 *S. aureus* SH1000 ⁴⁵ was grown to an optical density OD₆₀₀ of 1.0. Cells were harvested,
471 resuspended in distilled water, autoclaved and incorporated in agar plates at a final OD₆₀₀ of
472 0.5. Five μ l corresponding to serial dilutions of the recombinant lysostaphin proteins were
473 spotted on the plates containing autoclaved cells as a substrate and incubated overnight at
474 37 °C. Lytic activities were detected as clearing zones and compared by determining the lowest
475 amount of enzyme giving a detectable digestion of the substrate

476

477 **Data availability**

478 Structural data have been deposited in the Protein DataBank (PDB) with coordinate accession
479 numbers 6RK4 (high-resolution set) and 6RJE (home source set). All other data generated or
480 analyzed during this study are included in this published article (and its supplementary
481 information files) or are available from the corresponding authors on reasonable request.”

482

483 **References**

- 484 1. Schindler, C.A. & Schuhardt, V.T. Lysostaphin: a new bacteriolytic agent for the *Staphylococcus*.
485 *Proc Natl Acad Sci U S A* **51**, 414-21 (1964).
- 486 2. Schindler, C.A. & Schuhardt, V.T. Purification and properties of Lysostaphin--a lytic agent for
487 *Staphylococcus aureus*. *Biochim Biophys Acta* **97**, 242-50 (1965).
- 488 3. Thumm, G. & Götz, F. Studies on prolystaphin processing and characterization of the
489 lysostaphin immunity factor (Lif) of *Staphylococcus simulans* biovar *staphylolyticus*. *Mol*
490 *Microbiol* **23**, 1251-65 (1997).
- 491 4. Wu, J.A., Kusuma, C., Mond, J.J. & Kokai-Kun, J.F. Lysostaphin disrupts *Staphylococcus aureus*
492 and *Staphylococcus epidermidis* biofilms on artificial surfaces. *Antimicrob Agents Chemother* **47**,
493 3407-14 (2003).
- 494 5. Climo, M.W., Patron, R.L., Goldstein, B.P. & Archer, G.L. Lysostaphin treatment of experimental
495 methicillin-resistant *Staphylococcus aureus* aortic valve endocarditis. *Antimicrob Agents*
496 *Chemother* **42**, 1355-60 (1998).
- 497 6. Dajcs, J.J. *et al.* Lysostaphin treatment of methicillin-resistant *staphylococcus aureus* keratitis in
498 the rabbit. *Am J Ophthalmol* **130**, 544 (2000).
- 499 7. Johnson, C.T. *et al.* Hydrogel delivery of lysostaphin eliminates orthopedic implant infection by
500 *Staphylococcus aureus* and supports fracture healing. *Proc Natl Acad Sci U S A* **115**, E4960-E4969
501 (2018).
- 502 8. Kiri, N., Archer, G. & Climo, M.W. Combinations of lysostaphin with beta-lactams are synergistic
503 against oxacillin-resistant *Staphylococcus epidermidis*. *Antimicrob Agents Chemother* **46**, 2017-
504 20 (2002).
- 505 9. Kokai-Kun, J.F., Chanturiya, T. & Mond, J.J. Lysostaphin as a treatment for systemic
506 *Staphylococcus aureus* infection in a mouse model. *J Antimicrob Chemother* **60**, 1051-9 (2007).
- 507 10. Kokai-Kun, J.F., Walsh, S.M., Chanturiya, T. & Mond, J.J. Lysostaphin cream eradicates
508 *Staphylococcus aureus* nasal colonization in a cotton rat model. *Antimicrob Agents Chemother* **47**,
509 1589-97 (2003).
- 510 11. Satishkumar, R. *et al.* Evaluation of the antimicrobial activity of lysostaphin-coated hernia repair
511 meshes. *Antimicrob Agents Chemother* **55**, 4379-85 (2011).
- 512 12. Blazanovic, K. *et al.* Structure-based redesign of lysostaphin yields potent antistaphylococcal
513 enzymes that evade immune cell surveillance. *Mol Ther Methods Clin Dev* **2**, 15021 (2015).
- 514 13. Zhao, H. *et al.* Depletion of T cell epitopes in lysostaphin mitigates anti-drug antibody response
515 and enhances antibacterial efficacy *in vivo*. *Chem Biol* **22**, 629-39 (2015).
- 516 14. Liu, Y. *et al.* Immunomimetic designer cells protect mice from MRSA infection. *Cell* **174**, 259-
517 270 e11 (2018).
- 518 15. Raz, A., Serrano, A., Thaker, M., Alston, T. & Fischetti, V.A. Lysostaphin lysibody leads to
519 effective opsonization and killing of methicillin-resistant *Staphylococcus aureus* in a murine
520 model. *Antimicrob Agents Chemother* **62**:e01056-18.(2018).
- 521 16. Wall, R.J. *et al.* Genetically enhanced cows resist intramammary *Staphylococcus aureus* infection.
522 *Nat Biotechnol* **23**, 445-51 (2005).
- 523 17. Wittekind, M. & Schuch, R. Cell wall hydrolases and antibiotics: exploiting synergy to create
524 efficacious new antimicrobial treatments. *Curr Opin Microbiol* **33**, 18-24 (2016).
- 525 18. Baba, T. & Schneewind, O. Target cell specificity of a bacteriocin molecule: a C-terminal signal
526 directs lysostaphin to the cell wall of *Staphylococcus aureus*. *Embo J* **15**, 4789-97 (1996).
- 527 19. Lu, J.Z., Fujiwara, T., Komatsuzawa, H., Sugai, M. & Sakon, J. Cell wall-targeting domain of
528 glycylglycine endopeptidase distinguishes among peptidoglycan cross-bridges. *J Biol Chem* **281**,
529 549-58 (2006).
- 530 20. Mitkowski, P. *et al.* Structural bases of peptidoglycan recognition by lysostaphin SH3b domain.
531 *Sci Rep* **9**, 5965 (2019).

- 532 21. Gründling, A. & Schneewind, O. Cross-linked peptidoglycan mediates lysostaphin binding to the
533 cell wall envelope of *Staphylococcus aureus*. *J Bacteriol* **188**, 2463-72 (2006).
- 534 22. Tamai, E. *et al.* X-ray structure of a novel endolysin encoded by episomal phage phiSM101 of
535 *Clostridium perfringens*. *Mol Microbiol* **92**, 326-37 (2014).
- 536 23. Shaner, N.C. *et al.* A bright monomeric green fluorescent protein derived from *Branchiostoma*
537 *lanceolatum*. *Nat Methods* **10**, 407-9 (2013).
- 538 24. Williamson, M.P. *How proteins work*, 464 (Garland Science, New York, 2011).
- 539 25. Zhou, H.X. Quantitative relation between intermolecular and intramolecular binding of pro-rich
540 peptides to SH3 domains. *Biophys J* **91**, 3170-81 (2006).
- 541 26. Bolam, D.N. *et al.* *Pseudomonas* cellulose-binding domains mediate their effects by increasing
542 enzyme substrate proximity. *Biochem J* **331** (Pt 3), 775-81 (1998).
- 543 27. Gill, J. *et al.* The type II and X cellulose-binding domains of *Pseudomonas* xylanase A potentiate
544 catalytic activity against complex substrates by a common mechanism. *Biochem J* **342** (Pt 2), 473-
545 80 (1999).
- 546 28. Nagy, T. *et al.* Characterization of a double dockerin from the cellulosome of the anaerobic fungus
547 *Piromyces equi*. *J Mol Biol* **373**, 612-22 (2007).
- 548 29. Raghothama, S. *et al.* Characterization of a cellulosome dockerin domain from the anaerobic
549 fungus *Piromyces equi*. *Nat Struct Biol* **8**, 775-8 (2001).
- 550 30. Nega, M. *et al.* Secretome analysis revealed adaptive and non-adaptive responses of the
551 *Staphylococcus carnosus femB* mutant. *Proteomics* **15**, 1268-79 (2015).
- 552 31. Gally, D. & Archibald, A.R. Cell wall assembly in *Staphylococcus aureus*: proposed absence of
553 secondary crosslinking reactions. *J Gen Microbiol* **139**, 1907-13 (1993).
- 554 32. Gu, J. *et al.* Structural and biochemical characterization reveals LysGH15 as an unprecedented
555 "EF-hand-like" calcium-binding phage lysin. *PLoS Pathog* **10**, e1004109 (2014).
- 556 33. Meroueh, S.O. *et al.* Three-dimensional structure of the bacterial cell wall peptidoglycan. *Proc*
557 *Natl Acad Sci U S A* **103**, 4404-9 (2006).
- 558 34. Tossavainen, H. *et al.* Structural and Functional Insights Into Lysostaphin-Substrate Interaction.
559 *Front Mol Biosci* **5**, 60 (2018).
- 560 35. Francius, G., Domenech, O., Mingeot-Leclercq, M.P. & Dufrêne, Y.F. Direct observation of
561 *Staphylococcus aureus* cell wall digestion by lysostaphin. *J Bacteriol* **190**, 7904-9 (2008).
- 562 36. Jagielska, E., Chojnacka, O. & Sabala, I. LytM fusion with SH3b-like domain expands its activity
563 to physiological conditions. *Microb Drug Resist* **22**, 461-9 (2016).
- 564 37. Sabala, I. *et al.* Crystal structure of the antimicrobial peptidase lysostaphin from *Staphylococcus*
565 *simulans*. *FEBS J* **281**, 4112-22 (2014).
- 566 38. Mesnage, S., Chau, F., Dubost, L. & Arthur, M. Role of *N*-acetylglucosaminidase and *N*-
567 acetylmuramidase activities in *Enterococcus faecalis* peptidoglycan metabolism. *J Biol Chem* **283**,
568 19845-53 (2008).
- 569 39. Mesnage, S. *et al.* Molecular basis for bacterial peptidoglycan recognition by LysM domains. *Nat*
570 *Commun* **5**, 4269 (2014).
- 571 40. Kabsch, W. Xds. *Acta Crystallogr D Biol Crystallogr* **66**, 125-32 (2010).
- 572 41. McCoy, A.J. *et al.* Phaser crystallographic software. *J Appl Crystallogr* **40**, 658-674 (2007).
- 573 42. Zwart, P.H. *et al.* Automated structure solution with the PHENIX suite. *Methods Mol Biol* **426**,
574 419-35 (2008).
- 575 43. Emsley, P. & Cowtan, K. Coot: model-building tools for molecular graphics. *Acta Crystallogr D*
576 *Biol Crystallogr* **60**, 2126-32 (2004).
- 577 44. Joosten, R.P., Joosten, K., Cohen, S.X., Vriend, G. & Perrakis, A. Automatic rebuilding and
578 optimization of crystallographic structures in the Protein Data Bank. *Bioinformatics* **27**, 3392-8
579 (2011).

- 580 45. Horsburgh, M.J. *et al.* *sigmaB* modulates virulence determinant expression and stress resistance:
581 characterization of a functional *rsbU* strain derived from *Staphylococcus aureus* 8325-4. *J*
582 *Bacteriol* **184**, 5457-67 (2002).
583
584

585 **Acknowledgments**

586 LSG is a PhD student funded by the Mexican government through a CONACYT scholarship.
587 HWM is supported by a BBSRC MIBTP studentship. We thank BBSRC and EPSRC for
588 funding to upgrade the 600 and 800 MHz spectrometers, respectively (grant numbers
589 BB/R000727/1 and EP/S01358X/1). The work in IS laboratory is supported by the Foundation
590 for Polish Science (FNP) programme, co-financed by the European Union under the European
591 Regional Development Fund, grant TEAMTECH/2016-3/19.

592

593

594 **Authors' contribution**

595 SM conceived the project and designed experiments with MPW and ALL. AMH and AJR
596 assigned the SH3b spectrum. LSG carried out all NMR experiments and analysed them with
597 the help of AMH and MPW. BS and LSG built all SH3b recombinant proteins to carry out
598 functional assays and crystallographic analyses. AWM crystallised the protein and solved the
599 structure with the help of ALL. EJ and IS provided reagents. LSG, HWM, BS, AMH, MPW,
600 ALL and SM analyzed the data. LSG, SM, ALL and MPW wrote the manuscript.

601

602

603 **Figure legends**

604

605 **Figure 1. Mapping the interaction surface of the SH3b domain with synthetic *S. aureus***
606 **PG fragments**

607 For each NMR titration, the average CSP was calculated and two-fold average CSP was chosen
608 as a threshold to identify surface residues interacting with ligands. The residues interacting
609 with the pentaglycine crossbridges are highlighted in red, those interacting with the peptide
610 stem in green. Interaction maps corresponding to six ligands are shown. **a**, G5 peptide; **b**, P4;
611 **c**, P4-G5; **d**, P5-G5-P4; **f**, GM-P5-G5-GM-P4-G5. Titrations confirmed the existence of a
612 narrow cleft previously proposed to bind the PG crossbridges¹⁹ and recently shown to interact
613 with pentaglycine²⁰. They also revealed a set of residues interacting with the peptide stem,
614 located on the face of the protein opposite to the G5 binding cleft.

615

616 **Figure 2. Structure of lysostaphin SH3b in complex with the P4-G5 ligand**

617 The SH3b domain and a symmetry-related partner are coloured white and blue, respectively;
618 ligand is coloured by atom type, with P4 C atoms green and G5 C atoms pink. **a**, protein fold
619 with termini labelled, and two representations (fold and ligand in ribbon/stick and surface
620 formats). **b**, Co-crystal structure showing the SH3b:ligand shape complementarity. **c**, Rotated
621 view of a single SH3b domain showing the interaction with the P4 ligand (blue, with peptide
622 units labelled 1-4). **d**, experimental 2Fo-Fc difference map contoured at 1 σ for different
623 regions of the bound ligand, with selected interacting residues in stick form. The L-Ala 1 end
624 panel is from the 2.5 Å dataset, others are from the 1.4 Å form. Residues from the symmetry-
625 related SH3b domain are denoted by use of a prime ('), and hydrogen bonds represented as a
626 dashed line.

627

628 **Figure 3. Binding activity of recombinant SH3b-mNeonGreen (SH3b-NG) proteins to**
629 **purified *S. aureus* peptidoglycan**

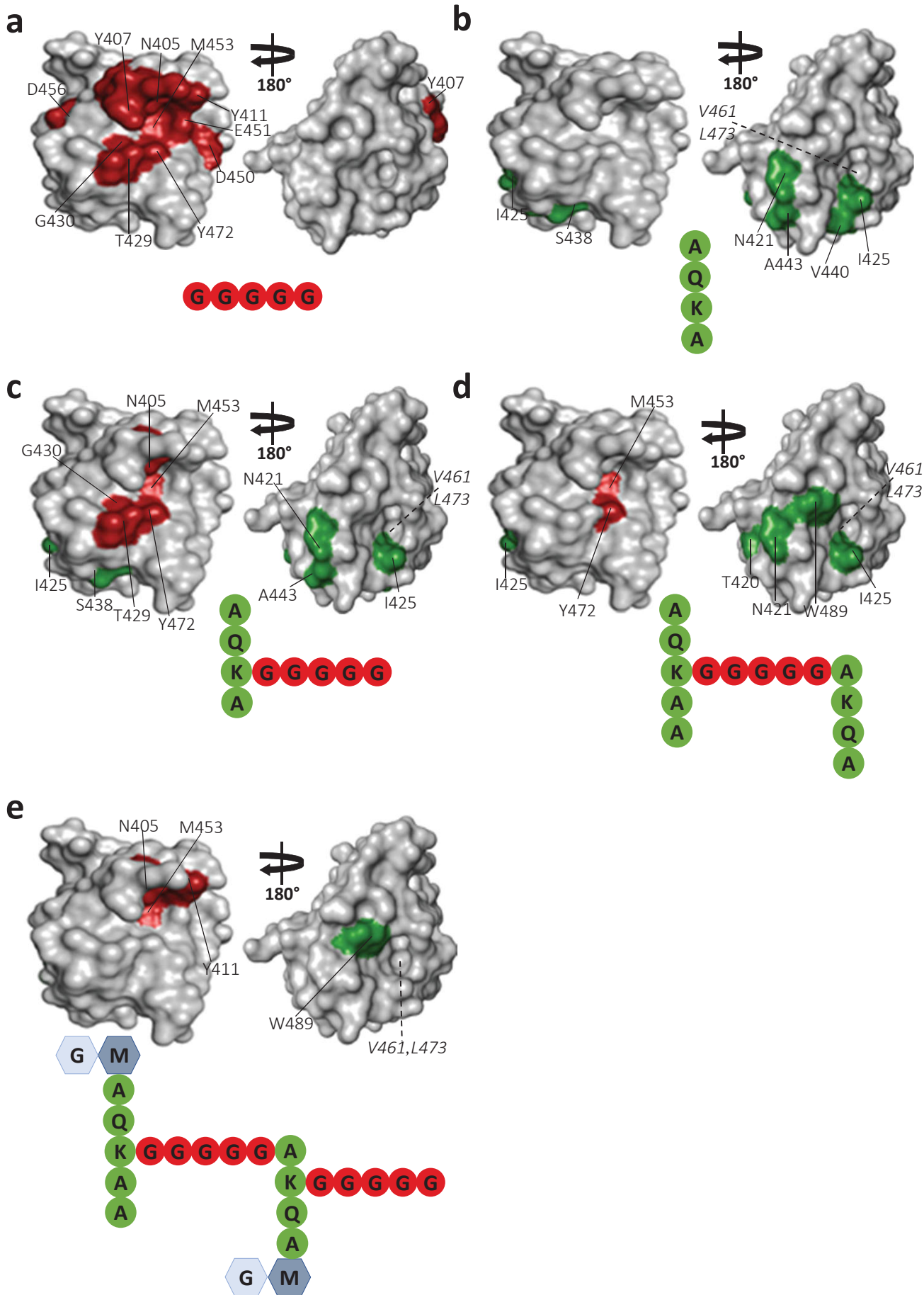
630 **a**, peptidoglycan binding activities of WT SH3b-NG on *S. aureus* WT and *fem* mutants with an
631 altered peptidoglycan crossbridge. **b**, peptidoglycan binding activities of WT SH3b-NG and
632 derivatives with mutations in residues involved in the interaction with the G5 ligand. **c**,
633 peptidoglycan binding activities of WT SH3b-NG and derivatives with mutations in residues
634 involved in the interaction with the P4 ligand. The graphs show dose-binding responses whilst
635 Supplementary Table 2 indicates the amount of PG required for 50% binding (PG₅₀) and the

636 corresponding fold change compared to the amount of PG required for 50% binding of the WT
637 protein as a reference.

638

639 **Figure 4. Models for binding of a ligand at two sites**

640 **a**, schematic representation of a receptor with two sites (R1 and R2), which bind the L1 and L2
641 ligand sites respectively. L1 and L2 are connected by a flexible linker. **b**, the flexibility of the
642 linker allows the R1 site to stay attached, but the R2 site to detach. The effective concentration
643 of L2 at the R2 site (and thus the cooperativity of binding) will depend on the length and
644 flexibility of the linker. **c**, if the linker is too short, it is not possible for the ligand to bind
645 simultaneously at both R1 and R2. It can alternate between both sites, which will still result in
646 cooperative binding, though less than in case **b**. **d**, a weaker enthalpy of binding (for example
647 due to the shortness of the linker preventing optimal binding at both sites) can to some extent
648 be compensated by greater entropy (increased relative motion of ligand and receptor) if there
649 is weak binding in non-optimal positions.



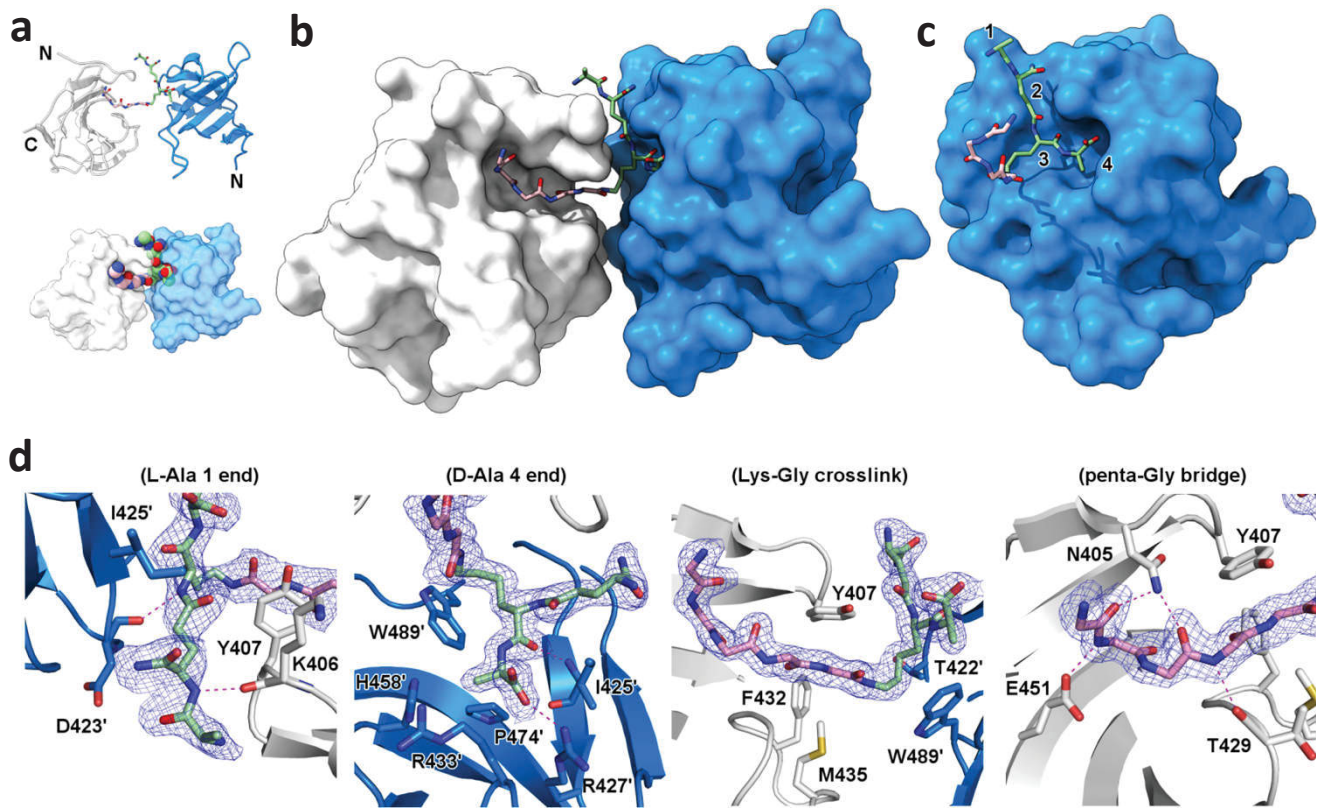


Figure 2

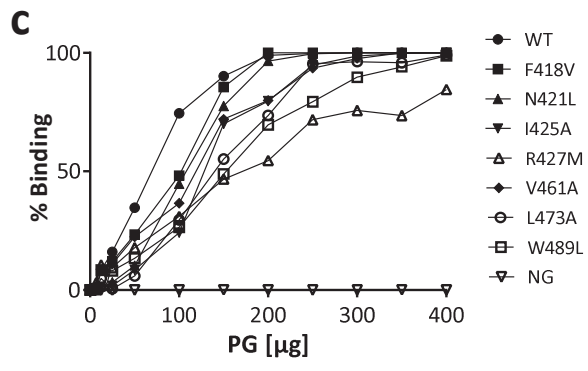
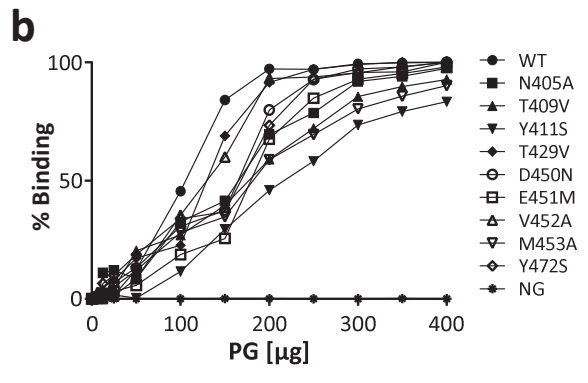
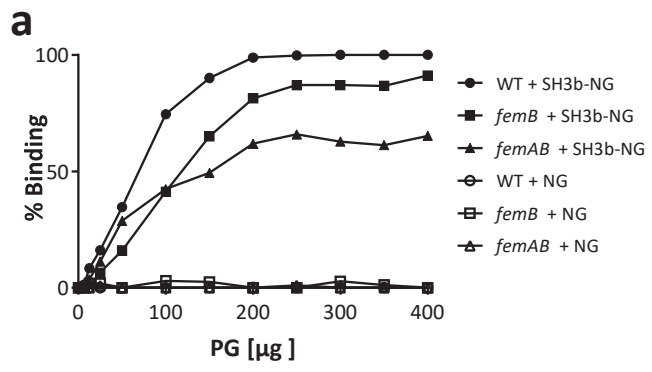


Figure 3

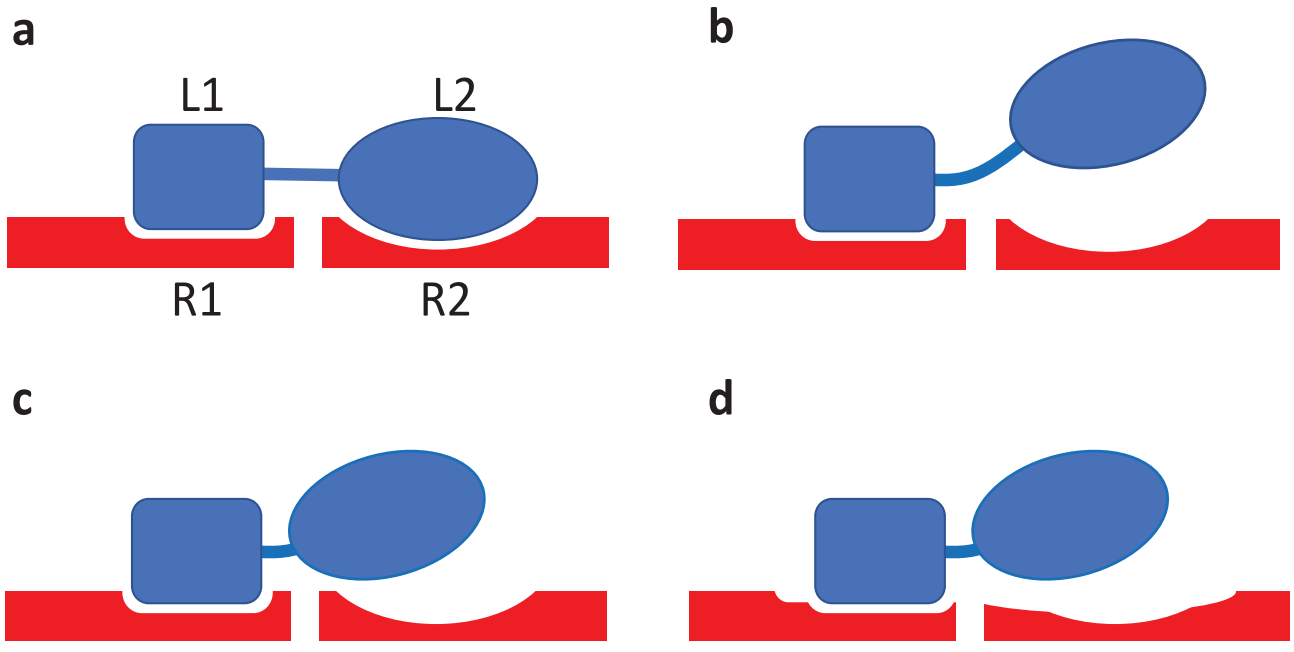


Figure 4

Supplementary Table 1. CSPs associated with amino-acid side-chains.

G5			P4		
Side chain	Normalized $\Delta\delta^a$ (ppm)	$\Delta\delta/\text{average}\Delta\delta^b$ (0.016)^c	Side chain	Normalized $\Delta\delta^a$ (ppm)	$\Delta\delta/\text{average}\Delta\delta^b$ (0.079)^c
Ws402	0.006	0.383	Ws402	0.039	0.489
N405s	0.122	7.643	N405s	0.028	0.350
Ws460	0.005	0.288	Rs427	0.168	2.122
Ws478	0.004	0.258	Rs433	0.048	0.610
Ws489	0.001	0.068	Ws460	0.143	1.796
			Rs470	0.038	0.484
			Rs476	0.015	0.194
			Ws478	0.014	0.175
			Ws489	0.157	1.982
P4-G5			GM-P4-G5		
Side chain	Normalized $\Delta\delta^a$ (ppm)	$\Delta\delta/\text{average}\Delta\delta^b$ (0.069)^c	Side chain	Normalized $\Delta\delta^a$ (ppm)	$\Delta\delta/\text{average}\Delta\delta^b$ (0.121)^c
Ws402	0.010	0.143	Ws402	0.126	1.045
N405s	*	*	N405s	0.174	1.446
Rs427	*	*	Rs427	0.226	1.873
Rs433	0.024	0.348	Rs433	0.096	0.794
Ws460	0.129	1.879	Ws460	0.199	1.648
Rs470	0.231	3.367	Rs470	0.216	1.786
Rs476	0.012	0.175	Rs476	0.071	0.588
Ws478	0.004	0.058	Ws478	0.021	0.171
Ws489	0.097	1.417	Ws489	0.143	1.188
P5-G5-P4-G5			GM-P5-G5-GM-P4-G5		
Side chain	Normalized $\Delta\delta^a$ (ppm)	$\Delta\delta/\text{average}\Delta\delta^b$ (0.119)^c	Side chain	Normalized $\Delta\delta^a$ (ppm)	$\Delta\delta/\text{average}\Delta\delta^b$ (0.057)^c
Ws402	0.059	0.499	Ws402	0.015	0.256
N405s	0.078	0.653	N405s	0.191	3.343
Rs427	0.244	2.059	Rs427	0.071	1.247
Rs433	0.132	1.108	Rs433	0.013	0.235
Ws460	0.189	1.597	Ws460	0.066	1.165
Rs470	0.083	0.703	Rs470	0.019	0.334
Rs476	0.032	0.272	Rs476	0.029	0.513
Ws478	0.172	1.452	Ws478	0.053	0.925
Ws489	0.095	0.802	Ws489	0.039	0.689

^a Normalized ¹H and ¹⁵N chemical shifts in ppm.

^b Value for the ¹H ¹⁵N chemical shift divided by the average chemical shift.

^c Average chemical shift value from all residues when titrated with the corresponding ligand.

*Slow conformational exchange was reported for the backbone and side-chain of these residues showing line broadening and disappearance of the signal at the highest ligand concentrations.

Supplementary Table 2. Peptidoglycan binding activities of WT SH3b-NG and derivatives showing the amount of PG required for 50% binding (PG₅₀) and the fold change as compared to the wild-type domain.

	SH3b	PG ₅₀	Fold change
Fig. 3a	WT ^c	69.2	1.00
	<i>femB</i>	118.3	1.71
	<i>femAB</i>	152.6	2.20
Fig. 3a	WT	105.8	1.00
	N405A	163.0	1.54
	T409V	167.3	1.58
	Y411S	193.5	1.83
	T429V	129.5	1.22
	D450N	164.8	1.56
	E451M	177.9	1.68
	V452A	129.7	1.23
	M453A	171.5	1.62
	Y472S	168.0	1.59
Fig. 3c	WT	69.2	1.00
	F418V	102.4	1.48
	N421L	107.9	1.56
	V461A	118.9	1.72
	I425A	128.1	1.85
	R427M	170.6	2.47
	L473A	139.0	2.01
	W489L	151.0	2.18

Table 3. Bacterial strains and plasmids used in this study

Strains, plasmids	Relevant properties or genotype ^a	Source or reference
Strains		
<i>Staphylococcus aureus</i>		
SH1000	8325-4 derivative with a restored <i>rsbU</i> allele	46
NCTC8325	Wild type strain	46
<i>Escherichia coli</i>		
Lemo21(DE3)	BL21 derivative for protein production	NEB
NEB5 α	Host strain for DNA cloning	NEB
Plasmids		
pET15b	Plasmid for the production of proteins with an N-terminal His-tag	Novagen
pET21a	Plasmid for the production of proteins with a C-terminal His-tag	Novagen
pET2818	Plasmid for the production of proteins with a C-terminal His-tag	lab stock
pET2817-TEV	Plasmid for the production of proteins with an N-terminal cleavable His-tag	lab stock
pET-SH3b	pET15b derivative encoding Lss SH3b domain for NMR experiments	38
pET-Lss	pET21a derivative for the expression of the full length Lss lysostaphin	39
pET-SH3b-TEV	pET2817-TEV derivative for the expression of the Lss-SH3b domain for X-ray crystallography	This study
pET-SH3b-NG	pET2818 derivative for the expression of SH3b-mNeonGreen fusions	This study

^a Amp^R, resistant to ampicillin; Erm^R, resistant to erythromycin

Supplementary Table 4. Oligonucleotides used in this study





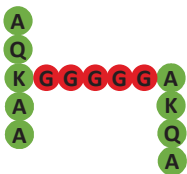
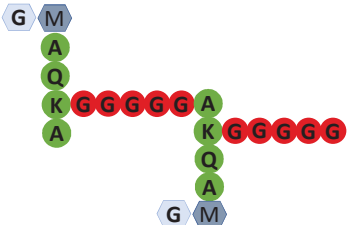
Name	Sequence
N405A_Fw	CATGGGATGGAAAACAGCCAAATATGGCACACTATATAAAATC
N405A_Rev	TAGTGTGCCATATTTGGCTGTTTTCCATCCCATGGTATATC
N405A_Fw_Lss	TACAGGTTGGAAAACAGCCAAATATGGCACACTATATAAAATC
N405A_Rev_Lss	AGTGTGCCATATTTGGCTGTTTTCCAACCTGTATTCGGCGTTG
T409V_Fw	ACAAACAAATATGGCGTGCTATATAAAATCAGAGTCAG
T409V_Rev	CTCTGATTTATATAGCACGCCATATTTGTTTGTTC
Y411S_Fw	AAATATGGCACACTATCAAAATCAGAGTCAGCTAGCTTC
Y411S_Rev	AGCTGACTCTGATTTTGATAGTGTGCCATATTTGTTG
F418V_Fw	CAGAGTCAGCTAGCGTCACACCTAATACAGATATAATAAC
F418V_Rev	ATCTGTATTAGGTGTGACGCTAGCTGACTCTGATTTATATAGTG
N421L_Fw	GCTAGCTTCACACCTCTTACAGATATAATAACAAGAACGAC
N421L_Rev	GTTATTATATCTGTAAGAGGTGTGAAGCTAGCTGACTC
I425A_Fw	ACCTAATACAGATATAGCAACAAGAACGACTGGTCCATTTAG
I425A_Rev	CCAGTCGTTCTTGTGGCTATATCTGTATTAGGTGTGAAGCTAG
T429V_Fw	ATAATAACAAGAACGGTTGGTCCATTTAGAAAGCATG
T429V_Rev	CTTCTAAATGGACCAACCGTCTTGTATTATATCTG
D450N_Fw	CAAACAATTCATTATAATGAAGTGATGAAACAAGAC
D450N_Rev	GTTTCATCACTTCATTATAATGAATTGTTTGACCTG
E451M_Fw	ACAATTCATTATGATATGGTGATGAAACAAGACGGTCATG
E451M_Rev	GTCTTGTTTCATCACCATATCATAATGAATTGTTTGAC
V452A_Fw	TTCATTATGATGAAGCGATGAAACAAGACGGTCATG
V452A_Rev	ACCGTCTTGTTCATCGCTTCATCATAATGAATTGTTTG
M453A_Fw	CATTATGATGAAGTGGCAAAAACAAGACGGTCATGTTTG
M453A_Rev	ATGACCGTCTTGTTCCTTCCACTTCATCATAATGAATTG
M461A_Fw	ACGGTCATGTTTGGGCAGGTTATACAGGTAACAGTG
M461A_Rev	TTACCTGTATAACCTGCCCAAACATGACCGTCTTGTTC
Y472S_Fw	AGTGGCCAACGTATTTCTTGGCTGTAAGAACATGGAAT
Y472S_Rev	TGTTCTTACAGGCAAGGAAATACGTTGGCCACTGTTAC
L473A_Fw	GGCCAACGTATTTACGCGCCTGTAAGAACATGGAATAAATC
L473A_Rev	CATGTTCTTACAGGCGCGTAAATACGTTGGCCACTGTTAC
W489L_Fw	ACTTTAGGTGTTCTTCTGGGAACTATAAAGGGATCCGGAG
W489L_Rev	TCCCTTTATAGTTCCCGAAGAACACCTAAAAGTATTAGTAG
W489L_Fw_Lss	TACTTTAGGTGTTCTTCTGGGAACTATAAAGCTCGAGCAC
W489L_Rev_Lss	GAGCTTTATAGTTCCCGAAGAACACCTAAAAGTATTAGTAG

Table 5. Data collection and refinement statistics

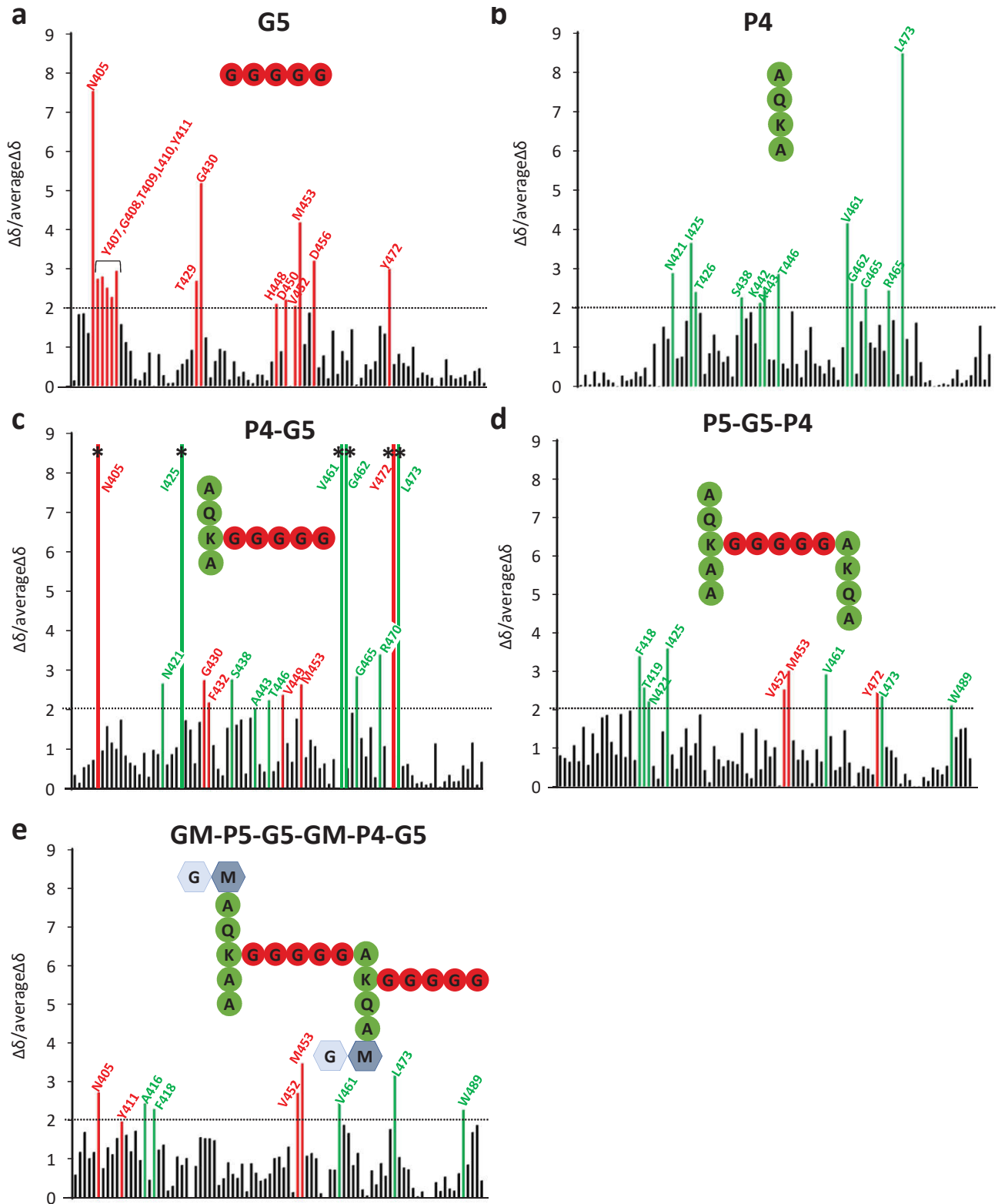
	Home source set	Synchrotron set
Data collection		
Space group	P4 ₁ 2 ₁ 2	P4 ₁ 2 ₁ 2
Cell dimensions		
<i>a</i> , <i>b</i> , <i>c</i> (Å)	47.2, 47.2, 123.1	47.1, 47.1, 122.4
α , β , γ (°)	90, 90, 90	90, 90, 90
Resolution (Å)	2.5(2.6-2.5)*	1.43 (1.47-1.43)
<i>R</i> _{merge}	12.8(21.5)	5.9 (341.3)
<i>I</i> / σ <i>I</i>	14.3(6.0)	21.6(1.1)
Completeness (%)	99.6(98.7)	98.9(98.4)
Redundancy	11.9(8.9)	24.3(24.7)
Refinement		
Resolution (Å)	2.5	1.43
No. reflections	5270	26342
<i>R</i> _{work} / <i>R</i> _{free}	25.4/29.0	19.9/23.0
No. atoms		
Protein	741	741
Ligand/ion	49	52
Water	3	24
<i>B</i> -factors		
Protein	27.7	43.4
Ligand/ion	29.7	44.2
Water	17.9	44.3
R.m.s. deviations		
Bond lengths (Å)	0.003	0.008
Bond angles (°)	1.18	1.49

A single crystal was used for both data collections.

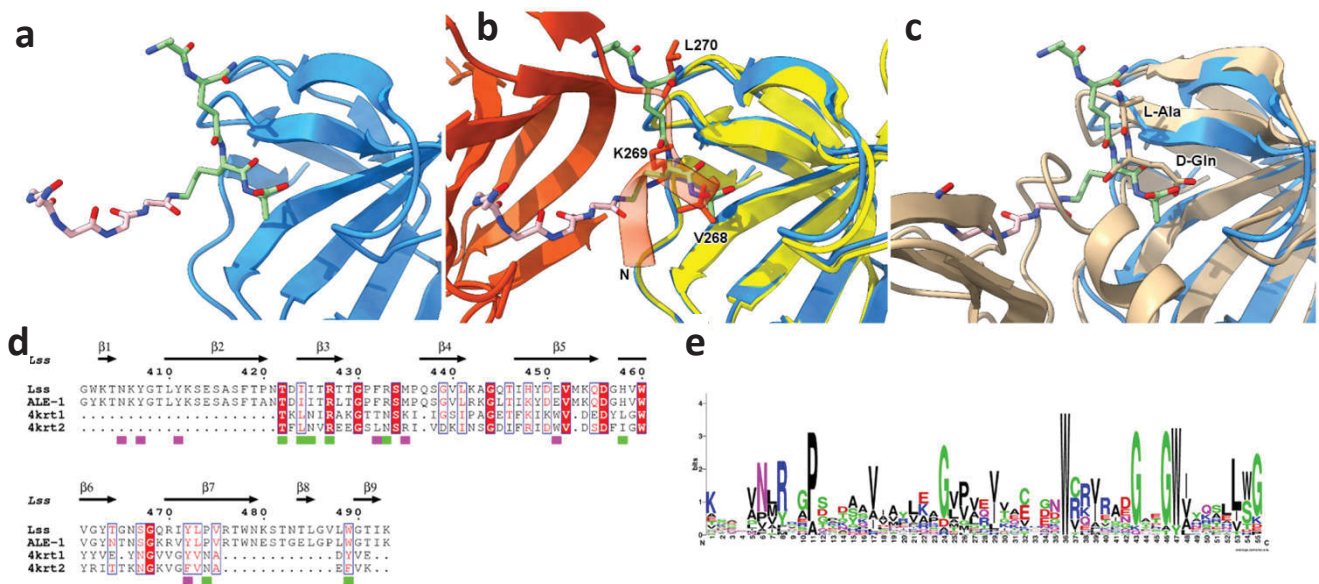
*Values in parentheses are for highest-resolution shell.

Ligand	Source
	GMGM Synthetic compound
	G5 Synthetic compound
	P4 Synthetic compound
	P4-G5 Synthetic compound
	P5-G5-P4 Synthetic compound
	GM-P5-G5-GM-P4-G5 Peptidoglycan digestion (mutanolysin)

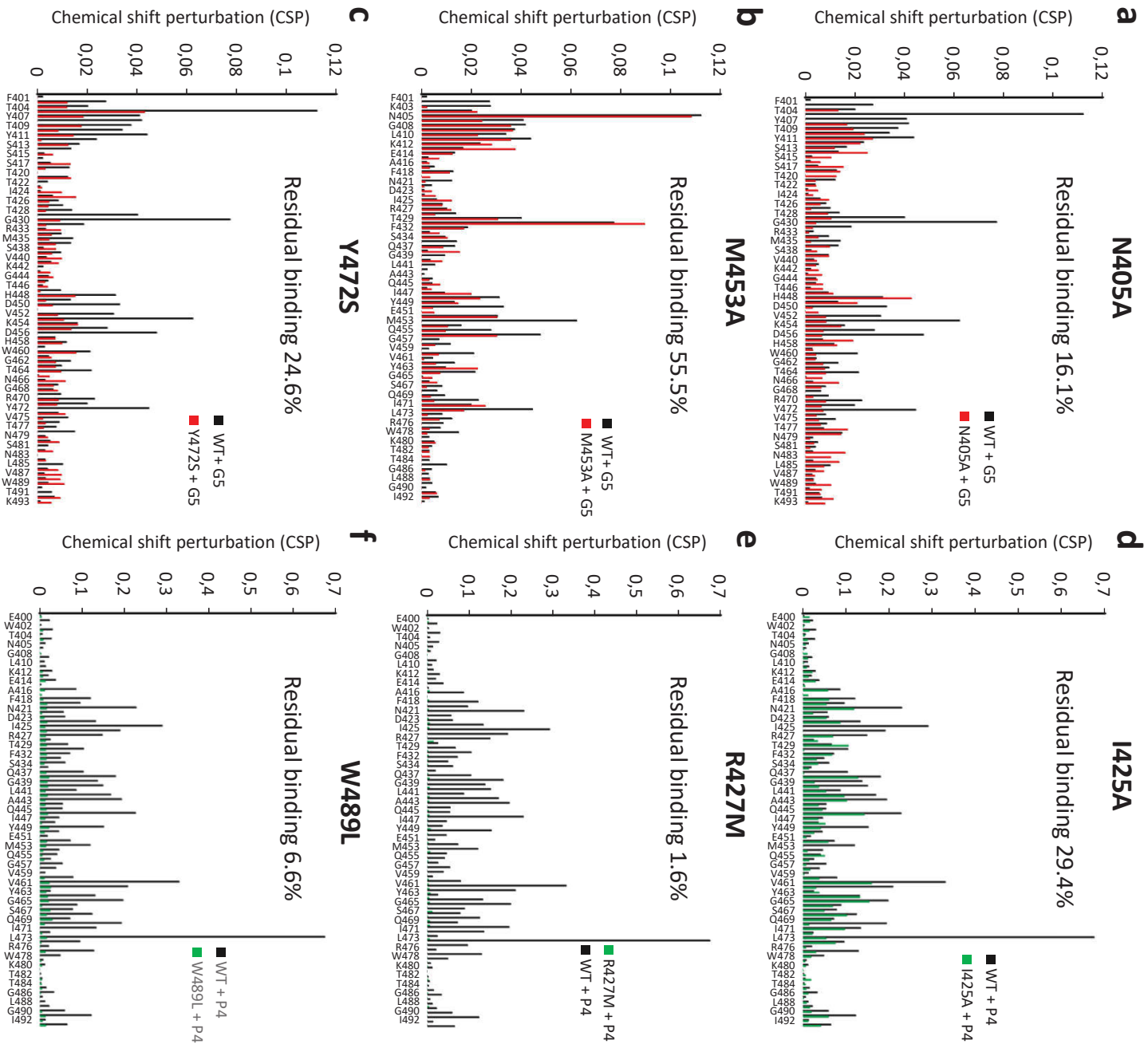
Supplementary Fig 1. *S. aureus* PG fragments used as SH3b ligands. The structure of each ligand, its name and method of preparation are indicated.



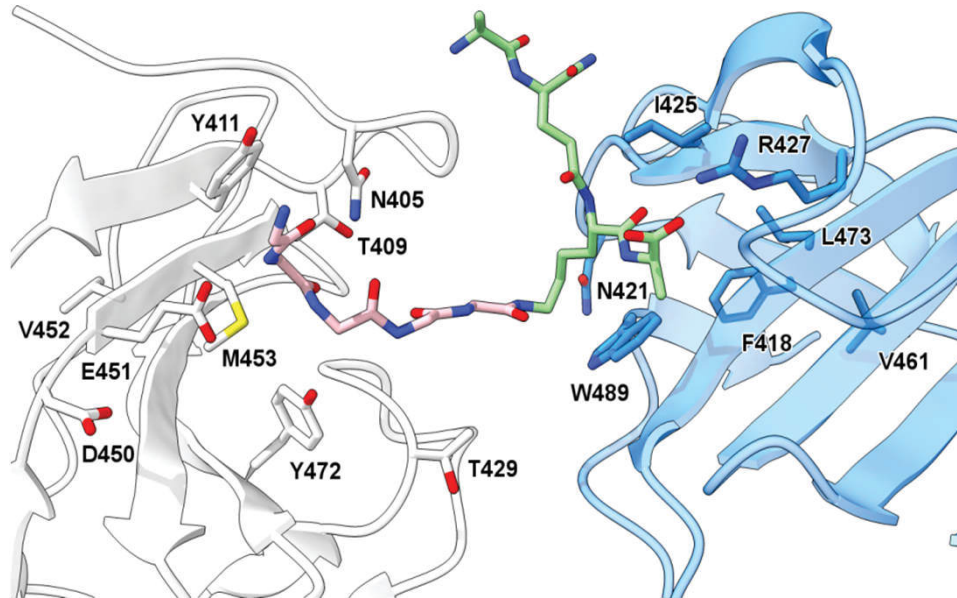
Supplementary Figure 3. Chemical shift perturbation (CSP) analysis of the SH3b protein interactions with a set of six different PG fragments derived from *S. aureus*. Histograms of the observed CSP values calculated as $\Delta\delta = (\Delta\delta H^2 + (0.154 \times \Delta\delta N)^2)$, as a function of the amino acid sequence are shown. The y-axis represents the ratio between individual CSPs and the average CSP (taking all residues into account). An arbitrary threshold of 2 was chosen. Residues associated with CSPs above the threshold using G5 as a ligand are in red, those with CSPs above the threshold using P4 as a ligand are in green. Titrations were carried out using 50 μM of protein and G5 (a), P4 (b), P4-G5 (c), P5-G5-P4 (d) and GM-P5-G5-GM-P4-G5 (e). 0, 0.33, 0.66, 1, 2, 4, 8, 16, 32, and 64 equivalents of ligand were used in (a)-(c); 16 equivalents in (d), and only 4 equivalents in (e) as protein aggregation occurred.



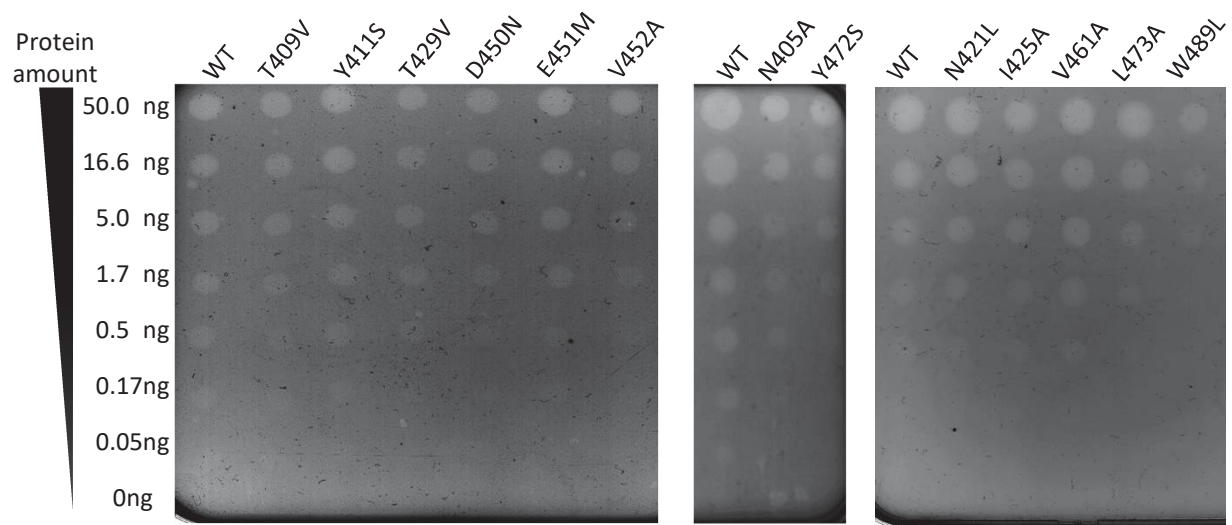
Supplementary Fig 4. Comparison of ligand-binding pocket to other SH3b structures and SH3 superfamily members. **a**, Lysostaphin SH3b domain in complex with the P4-G5 ligand. **b**, Superimposition of the structure shown in A onto the ALE-1 structure (1r77, two symmetry-related monomers orange and yellow). The P4-G5 ligand occupies the same space as an affinity purification tag (helical turn, N-terminus labelled). **c**, Superimposition of the structure shown in A onto the phi7917 structure (5D76, tan). Ligand P3(K)-P4(A) are sterically equivalent to tag residues K269 and V268, respectively. The phi7917 ligand (L-Ala-D-Gln) is positioned with its peptide bond over the P3-P4 peptide. **d**, Sequence alignment of Lysostaphin SH3b (SH3_5 subfamily) with ALE-1 (SH3_5) and the two tandem domains of *Clostridium* phage phiSM101 (4krt, SH3_3 subfamily), G5 and P4-ligating residues annotated with magenta and green block below text, respectively. **e**, Weblogo (Crooks *et al.*, 2004) plot of sequence consensus of SH3_4 subfamily, identifying features with likely equivalence to SH3_3 and SH3_5 alignment: NxR (position 6-8, match Lss I425-R427), W (36, match to W460), GxxGW (43-47, match to G468-Y472) and LWG (53-55, match to L488-G490). No structures are currently available for SH3_4 proteins, but structural comparison between Lss/ALE-1 and 4krt confirms conservation of the P-stem D-Ala(4)-carboxylate pocket.



Supplementary Fig 5. Comparison of chemical shift perturbations (CSP) in wild-type and SH3b mutant domains associated with the binding to G5 and P4 ligands. Histograms show individual CSP values from the ^{15}N -HSQC titrations of N405A (a), M453A (b), and Y472S mutants (c) in red compared to the CSP values from the WT protein (in grey) following addition of 32 equivalents of G5. (c), (d) and (e) show CSPs from titrations of I425A, R427M and W489L, respectively (in green) compared to CSP values from the WT protein (in grey) following addition of 32 equivalents of P4. The percentage of residual binding activity deduced from the average CSP values is indicated.



Supplementary Fig 6. Mutagenized residues at the SH3b:P4-G5 interaction interface. The representation is identical to figure 2, but displaying all residues selected for mutation in stick form (to avoid confusion, residues are only displayed once, from the SH3b domain that places them closest to the ligand).



Supplementary Fig 7. Comparison of the enzymatic activity of lysostaphin (Lss) recombinant proteins containing mutations in the SH3b domain. Three independent series of purifications were carried out (left, middle and right panels), each including a wild-type protein as a control. Five μ l corresponding to serial dilutions of recombinant Lss proteins were spotted on agar plates containing autoclaved *S. aureus* cells (final OD_{600} of 1) as a substrate. Lytic activities were detected as clearing zones and compared by determining the lowest amount of enzyme giving a detectable digestion of the substrate.

N-terminally His-tagged SH3b (pET-SH3b) for NMR analyses; residues 402-493

MGHHHHHHEFWKTNKYGTLYKSESASFTPNTDIITRTTGPFRSMPQSGVLKAGQTIHYDEVMKQDG
HVWVGYTGNSGQRIYLPVRTWNKSTNTLGVLWGTIK

N-terminally His-tagged SH3b (pET-SH3b-TEV) for X-ray crystallography; residues 402-493

MSGHHHHHHAMGENLYFQG^SWKTNKYGTLYKSESASFTPNTDIITRTTGPFRSMPQSGVLKAGQTIH
YDEVMKQDGHVWVGYTGNSGQRIYLPVRTWNKSTNTLGVLWGTIKVLWGTIK

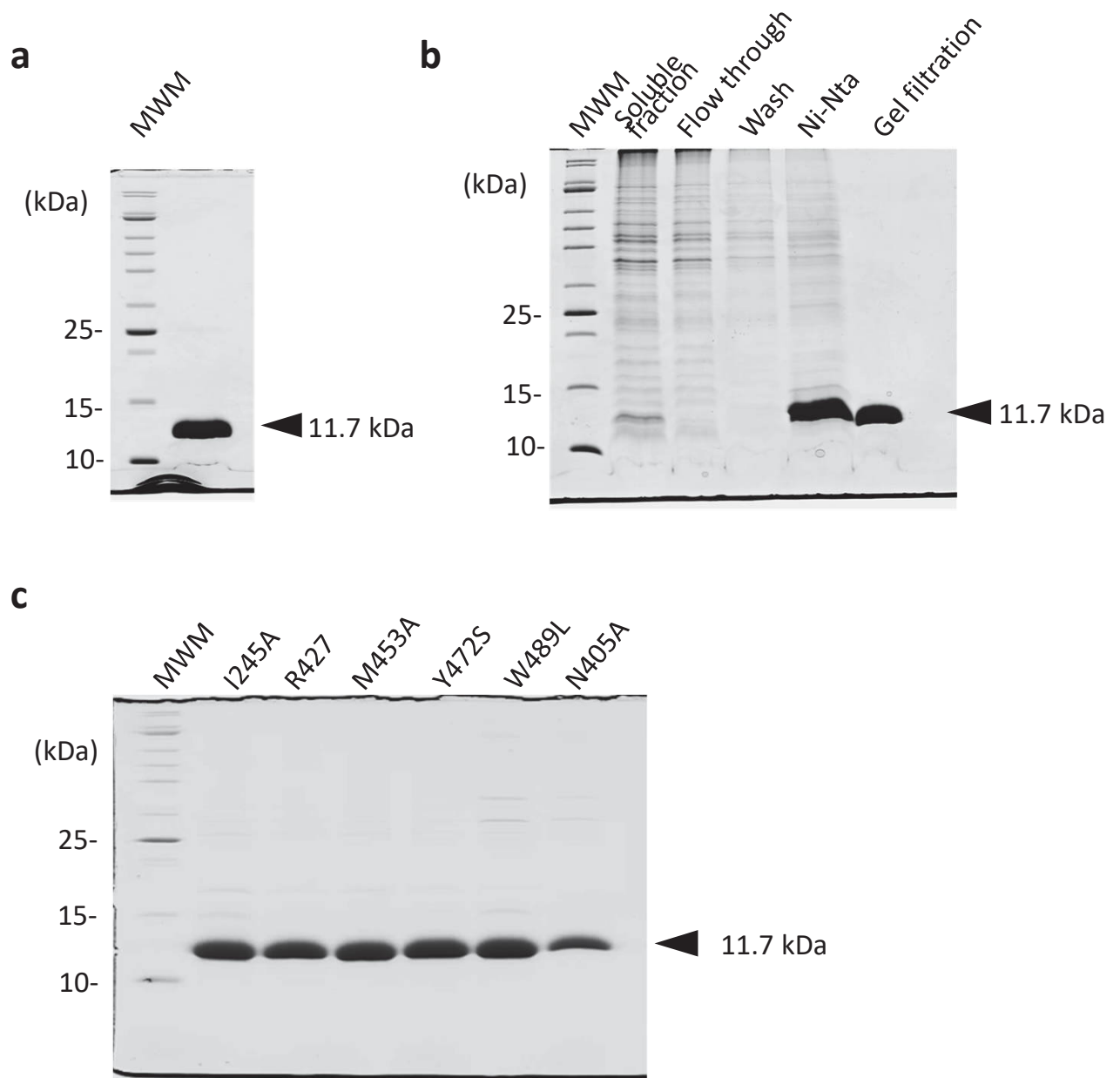
C-terminally his-tagged SH3b-mNeonGreen fusion (pET-SH3b-NG) for binding assays; residues 401-493

MGWKTNKYGTLYKSESASFTPNTDIITRTTGPFRSMPQSGVLKAGQTIHYDEVMKQDGHVWVG
YTGNSGQRIYLPVRTWNKSTNTLGVLWGTIKGSGGSGSGSNNSGMVSKGEEDNMASLPATHELHIFGSI
NGVDFDMVGQGTGNPNDGYEELNLKSTKGLQFSPWILVPHIGYGFHQYLPYPDGMSPFQAAMVD
GSGYQVHRTMQFEDGASLTVNYRYTYEGSHIKGEAQVKGTGFPADGPVMTNSLTAADWCRSKKTYPN
DKTIISTFKWSYTTGNGKRYRSTARTTYTFAKPMAANYLKNQPMYVFRKTELKHSKTELNFKEWQKAFT
DVMGMDELYKHHHHHHH

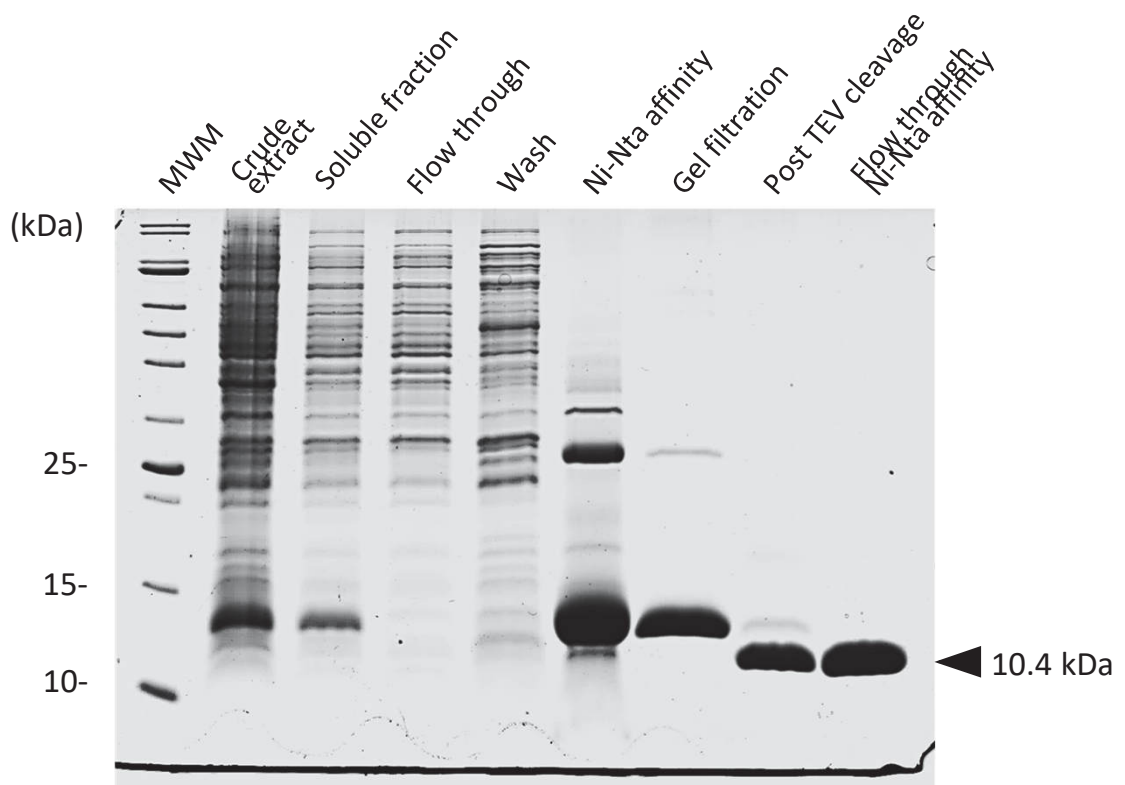
Full length lysostaphin (pET-Lss) for activity assays; residues 248-493

MAATHEHSAQWLNNYKKGYGYPYPLGINGGMHYGVDFFMNIGTPVKAISSGKIVEAGWSNYGGG
NQIGLIENDGVHRQWYMHLKYNVKGVDYVKAGQIIGWSGSTGYSTAPHLHFQRMVNSFSNSTAQD
PMPFLKSAGYGKAGGTVTPNTGWKTNKYGTLYKSESASFTPNTDIITRTTGPFRSMPQSGVLKAGQ
TIHYDEVMKQDGHVWVGYTGNSGQRIYLPVRTWNKSTNTLGVLWGTIKLEHHHHHHH

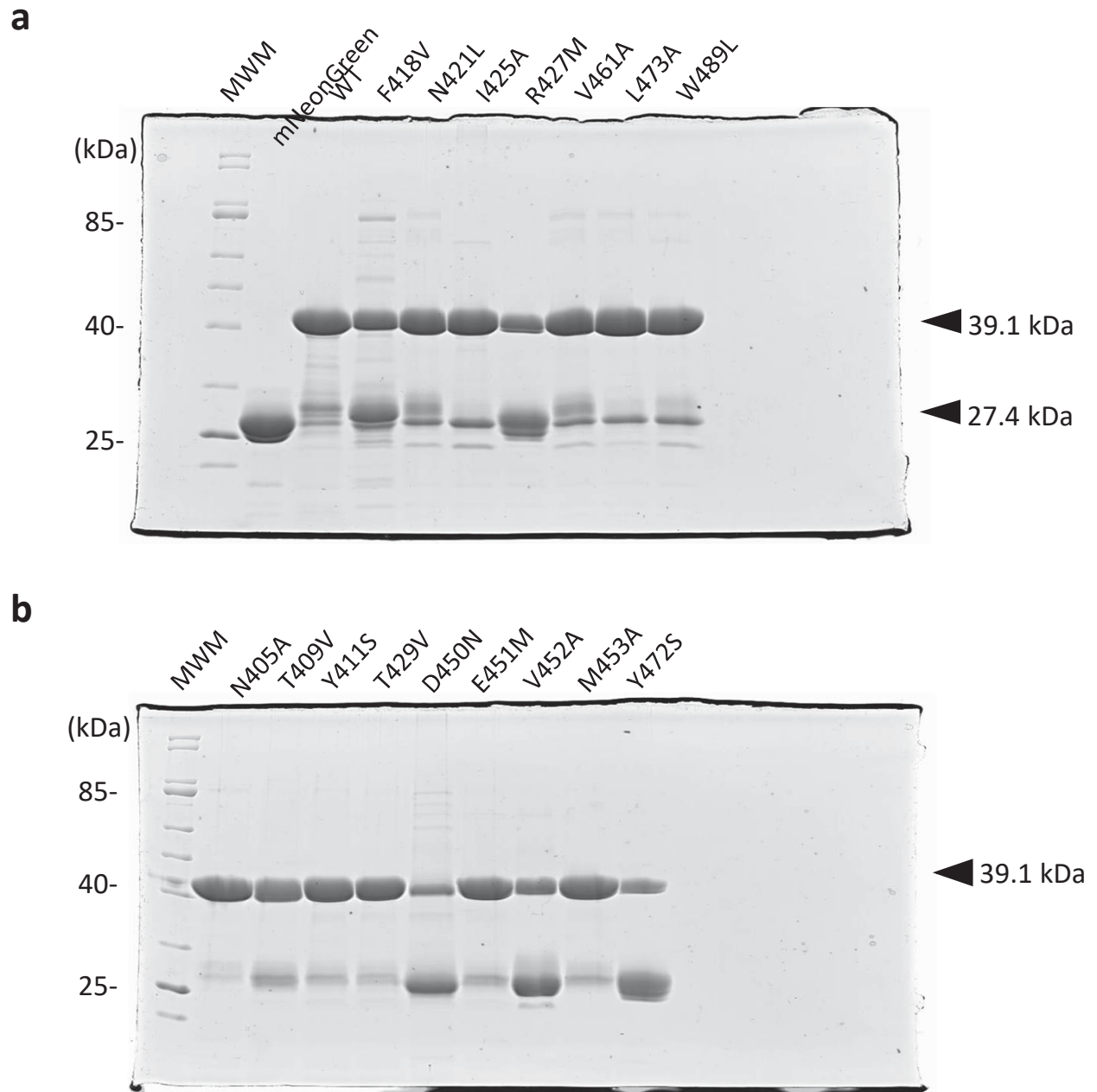
Supplementary Fig 8. Amino acid sequences of the recombinant wild-type proteins used in this study. In each case, both the plasmid encoding the recombinant SH3b protein (in brackets) and the experiment it was used for are indicated. The SH3b domain is in red, amino acids encoded by the expression vector in grey, linker in blue and mNeonGreen in green. The TEV cleavage site is indicated by an arrow.



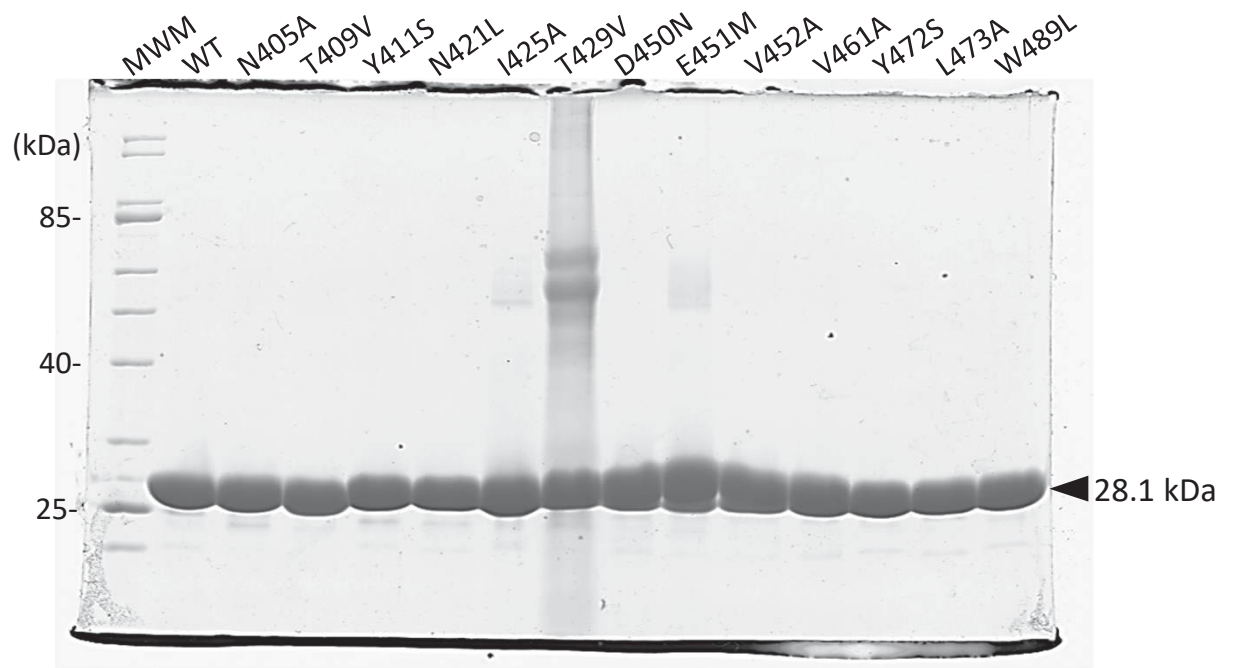
Supplementary Fig 9. SDS-PAGE analysis of recombinant proteins used for NMR studies. **a**, doubly labelled SH3b domain for spectrum assignment described in Supplementary Fig. 2. **b**, singly labelled His-tagged SH3b domain used for NMR titrations with ligands described in Fig. 1 and Supplementary Fig. S3. **c**, singly labelled His-tagged derivatives used for the mutational analysis of the SH3b domain described in Supplementary Fig. 5.



Supplementary Fig 10. SDS-PAGE analysis of recombinant proteins used for X-ray crystallography. The different steps of the purification are described. The final purification product corresponding to the SH3b domain without any His-tag was used for co-crystallisation experiments.



Supplementary Fig 11. SDS-PAGE analysis of recombinant SH3bp-mNeonGreen fusion proteins used for PG binding assays. a, mNeonGreen control and SH3b mutants harbouring mutations in the residues involved in the interaction with G5 ligands. **b,** SH3b mutants harbouring mutations in the residues involved in the interaction with P4 ligands. The amount of protein per binding assay was adjusted using the fluorescent signal intensity of the full-length protein.



Supplementary Fig 12. SDS-PAGE analysis of recombinant SH3bp-mNeonGreen fusion proteins used for PG binding assays. a, mNeonGreen control and SH3b mutants harbouring mutations in the residues involved in the interaction with G5 ligands. b, SH3b mutants harbouring mutations in the residues involved in the interaction with P4 ligands. The amount of protein per binding assay was adjusted using the fluorescent signal intensity of the full-length protein.